PROCEDURAL AND DOSIMETRIC ASPECTS IN PERIPHERAL ANGIOGRAPHY USING CO$_2$ AS CONTRAST MEDIUM

Relatore:
Prof.
Romano Zannoli

Correlatore:
Dott.
David Bianchini

Presentata da:
Manami Zanzi

Abstract

Lo scopo di questa tesi è lo studio degli aspetti procedurali e dosimetrici in angiografie periferiche che utilizzano la CO_2 come mezzo di contrasto.

La tecnica angiografica consiste nell'imaging radiologico di vasi sanguigni tramite l'iniezione di un mezzo di contrasto, e il suo uso è in costante incremento a causa dell'aumento di pazienti con malattie vascolari. I mezzi di contrasto iodati sono i più comunemente utilizzati e permettono di ottenere immagini di ottima qualità, ma presentano il limite di una elevata nefrotossicità. La CO_2 è considerata un'interessante alternativa al mezzo iodato, per la sua acclarata biocompatibilità, soprattutto per pazienti con elevati fattori di rischio (diabete e/o insufficienza renale). Il suo utilizzo presenta comunque alcuni aspetti problematici, dovuti allo stato gassoso e al basso contrasto intrinseco rispetto alla soluzione iodata. Per quest'ultimo motivo si ritiene generalmente che l'utilizzo della CO_2 comporti un aumento di dose rispetto ai mezzi di contrasto tradizionali.

Il nostro studio, effettuato su diversi apparati radiologici, ha dimostrato che i parametri di emissione radiologica sono gli stessi per i protocolli di angiografia tradizionale, con iodio, e quelli che utilizzano CO_2. Questa evidenza suggerisce che i protocolli CO_2 operino solo sul trattamento delle immagini ottenute e non sulla modalità di acquisizione, e dal punto di vista dosimetrico l'angiografia con CO_2 è riconducibile all'angiografia tradizionale. L'unico fattore che potrebbe portare a un effettivo incremento di dose al paziente è un allungamento dei tempi di scopia e di procedura, che andrebbe verificato con una campagna di misure in ambito clinico.

Sulla base della stessa evidenza, si ritiene che la visualizzazione della CO_2 possa essere ulteriormente migliorata attraverso l'ottimizzazione dei parametri di emissione radiologica (kVp, frame rate e durata degli impulsi) attualmente predisposti per l'uso di mezzi di contrasto iodati.

II

Contents

Introduction

Angiography is an important radiological imaging technique that allows the visualization of blood vessels through the injection of a contrast medium. Peripheral angiography, in particular, is a powerful instrument for the treatment of vascular diseases. However, an increasing number of patients presents high risk factors for the use of traditional iodinated contrast media. These include diabetes, renal diseases, allergies and very young or old age.

Carbon dioxide represents an interesting alternative for these patients, thanks to its lack of allergic reactions and renal toxicity. Along with a number of advantages, however, the use of a gaseous contrast media entails a series of technical issues. Difficulties in controlling its delivery and the risk of air contamination could be reduced through the introduction of innovative delivery systems, such as automatic injectors. Because of its X-ray absorption characteristics, CO_2 provides less contrast than iodinated contrast media, and for this reason it is generally believed to require higher doses than traditional angiographies.

In this work we addressed the dosimetric aspects of CO_2 angiography by studying the image acquisition protocols for both traditional and CO_2-based peripheral angiography on different fluoroscopy equipment.

The first chapter gives an overview of the problem, briefly introducing the angiographic technique, contrast media, fluoroscopy systems and some basic notions on radiological protection in medical exposures. The second chapter is devoted to the presentation of the considered instrumentation, while in the following chapters we illustrate and discuss the results of our measures.

1

CHAPTER 1

Overview of the problem

1.1   Angiography

Angiography is a medical imaging technique performed to visualise blood vessels, in order to detect eventual abnormalities or blockages throughout the circulatory system and in some organs. The procedure is commonly used to identify conditions that affect the vessels and the blood flow, such as atherosclerosis, heart diseases or aneurysms, to give surgeons an accurate "map" of blood vessels prior to surgery, and many other applications.

Angiographies have a fundamental role in interventional radiology (IR), the branch of radiology that comprises image-guided therapeutic interventions. Over the last few decades this field has become increasingly important, and the types and complexity of the procedures have greatly expanded [1]. Angiograms are routinely performed during interventional radiology procedures, to guide the radiologist in the insertion of catheters, guidewires and stents.

The angiographic technique has multiple applications, such as abdominal angiographies, cerebral angiographies and peripheral angiographies [2]. In particular, peripheral angiography is a steadily growing field, due to the increase of the number of patients with Peripheral Vascular Disease. PVD is a very common condition that usually develops as a result of atherosclerosis, a hardening of the arteries that occurs when cholesterol and scar tissue build up. The clogged arteries cause decreased blood flow to the legs, which can result in pain when walking and, if not properly treated, could eventually lead to gangrene and amputation.

1.1.1   Angiographic procedures

Angiographies require an adequate patient preparation. If the patient has a history of contrast allergy or renal failure, an appropriate preparation with steroid and hydration is usually recommended. Anaesthesia is avoided since patients have to remain alert during the examination, so that they can cooperate in holding their breath when needed, as respiratory motion might contribute to motion blurring in the final images. Sedatives and analgesics are instead used to alleviate the discomfort of the procedure and reduce anxiety and restlessness.

Patients are precautionarily monitored throughout the procedure, generally with pulse oximetry, ECG, heart rate, respiratory rate and blood pressure.

To perform the angiogram, the doctor inserts a catheter into the blood vessel through a small incision or a wide needle. Depending on the purpose of the procedure the insertion is made in different body parts, though the most commonly used is the femoral artery. With the help of X-ray imaging, the catheter is then carefully moved to the interested area.

Once the catheter is in place, angiographic image acquisition can start and the radiologist injects a contrast agent through the catheter. In fact, as both blood and soft tissues have a similar X-ray attenuation coefficients, a contrast agent is necessary to outline the vessels. The choice of this contrast medium is quite relevant and requires a careful evaluation of the contrastographic efficiency, the risks of adverse effects and also the cost.

Angiographic images are generally produced using a technique called *digital subtraction angiography* (DSA), that shows only the contrast-filled vessels while suppressing other anatomical features such as bones and other organs. While being extremely effective in most cases, DSA requires the patient to remain motionless, hence it cannot be used for the heart. For procedures like coronary angiography it is fundamental to use high frame rates, in order to reduce motion blurring.

In the case of IR procedures, the interventional radiologist can treat the patient without surgery at the same time the angiogram is performed.

During the procedure, both fluoroscopy and radiography are performed, according to the different instances. For example, fluoroscopy is used for a live monitoring of the catheter while radiography is mainly used to take good-quality images for the patient's medical record.

Digital subtraction angiography

This technique increases the contrast of the blood vessels and reduces anatomical noise by subtracting an image acquired before injecting the contrast media (mask) to the images acquired after the injection. All the images undergo a log transform before subtraction, in order to obtain a final image in which the signal only depends on the amount of contrast in the vessel and not on the background.

Assuming that the patient has a thickness x_t and a linear attenuation coefficient of μ_t, the mask image can be modeled as:

$$I_m = \alpha I_0 e^{-\mu_t x_t}$$

where I_0 is the photon fluence of the unattenuated radiation and α is a conversion factor which relates image signal and photon fluence. This equation derives from the Beer–Lambert law, hence it is only approximately correct as the radiation is not monochromatic.

After the contrast injection, we consider a vessel of thickness x_I (where $x_I \ll x_t$) and linear attenuation coefficient of μ_I. The obtained image is:

$$I_I = \alpha I_0 e^{-(\mu_t x_t + \mu_I x_I)}$$

If these images where linearly subtracted, the outcome would be an image with this form:

$$S_{lin} = I_m - I_I = \alpha I_0 e^{-(\mu_t x_t)} \left[1 - e^{-(\mu_I x_I)} \right]$$

Assuming that the signal of the vessel is so small that $\mu_I x_I << 1$, we have:

$$S_{lin} = \alpha (\mu_I x_I) I_0 e^{-(\mu_t x_t)}$$

Therefore, using linear subtraction, we obtain an image in which the vessel thickness x_I is modulated by the patient thickness x_t.

On the other hand, logarithmic subtraction does not retain such anatomical structure. In fact the resulting image has this form:

$$S_{log} = ln(I_m) - ln(I_I) \cong [-\mu_t x_t] - [-\mu_t x_t - \mu_I x_I] = \mu_I x_I$$

showing that the signal is not affected by the patient thickness or the anatomy on which the opacified artery is superimposed.

The major source of artefacts in DSA is patient motion between the capture of the different images. In some cases these artifacts can be reduced through the use of processing techniques, such as pixel shifting of the mask image.

1.1.2 Iodinated contrast media (ICM)

The most commonly used contrast media are iodine-containing. These are classified as positive contrast media, as they have a high atomic number and appear more radiopaque than the surrounding tissues.

Currently used ICM are triiodinated benzoic acid derivatives, and can be differentiated according to their physicochemical properties (iodine content, osmolarity, level of ionization and degree of polymerization). ICMs can be divided in four groups: ionic monomers, non-ionic monomers, ionic dimers, and non-ionic dimers (fig.1.1)
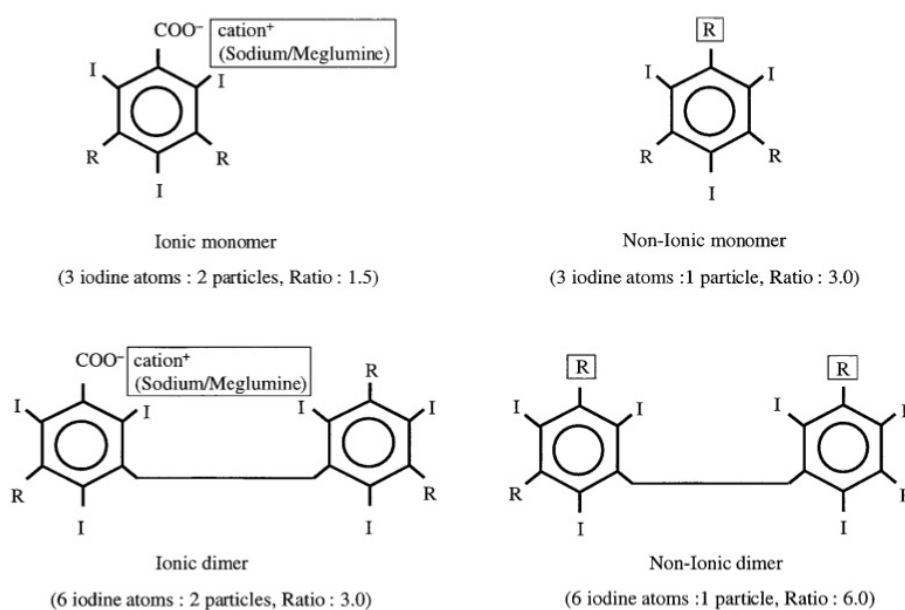
Figure 1.1: Classification of iodinated contrast agents [4].

The iodine to particle ratio is important, as it defines the relationship between contrastographic efficacy and osmotic effect.

Ionic monomers have a low iodine-to-particle ratio, 1.5, and are thus classified as *high-osmolar contrast media* (HOCM). These are the most traditional ICM, and are still in use because of their relatively low cost.

Both non-ionic monomers and ionic dimers have a ratio of 3, and are known as *low-osmolar contrast media* (LOCM).

The newest ICM are non-ionic dimers which have a ratio of 6, and are called *iso-osmolar contrast media* (IOCM) as their osmolarity similar to that of blood plasma.

While HOCM are known to be more nephrotoxic than the others [3], it is

still unclear whether all LOCM and IOCM have similar toxicities or not. In particular, IOCM are not as safe as originally hoped, probably due to their high viscosity.

Most of the contrast media is eliminated via the kidneys, and the elimination half-life following intravascular administration is about 2 hours in patients with normal renal function. In patients with renal impairment, on the other hand, the excretion time is prolonged and can last for several weeks [4]. The administration of iodinated contrast media can cause side effects in 7-8% of cases, with severe adverse reactions in 0.1% of patients [3].
The majority of these side effects are unpredictable and not dose-dependent, and they can be classified as acute (if they occur immediately after the injection) or delayed (if they appear after more than 1 hour but within 7 days of contrast injection).
Acute contrast reactions can range from minor effects, that are usually of short duration and do not require specific treatment (e.g. flushing, nausea, pruritus, vomiting and headache), to severe and life-threatening reactions such as convulsions, unconsciousness, laryngeal oedema, severe bronchospasm, pulmonary oedema, severe cardiac dysrhythmias and arrest, and cardiovascular and pulmonary collapse.
Delayed reactions are generally mild and include fever, rash, flushing, dizziness, pruritus, arthralgia, diarrhoea, nausea, vomiting, headache and occasionally hypotension. Nevertheless, there have been cases of serious delayed reactions (e.g. shock, hypotension, angio-oedema and dyspnoea).
There are several predisposing factors that can increase the incidence of severe contrast reactions, such as very young or old age, a history of allergy or asthma and cardiac or renal disease.

A very important side effect due to the administration of contrast media is the "*contrast medium nephrotoxicity*" (CMN), which is a reduction in renal function in the absence of an alternative aetiology. Most episodes are self-limiting and resolve within 1 or 2 weeks, and permanent renal damage is rare.
The incidence of CMN is low in patients with normal renal function (from 0% to 10%) but it increases in patients with renal problems (ranging from 12% to 27%, as reported by several studies [4]). There are some known factors that increase the risk of developing CMN: pre-existing renal impairment, as stated above, especially when this reduction in renal function is secondary to diabetic nephropathy; large doses of ICM; administration of ICM in the renal arteries; dehydration; congestive cardiac failure; old age (over 70 years); and the concurrent use of nephrotoxic drugs. The type of ICM also makes a

difference, as high-osmolarity ICM are more nephrotoxic than those with a lower osmolarity [6].

In patients with risk factors it is therefore important to take some measures to reduce the severity of CMN, such as extracellular volume expansion (e.g. intravenous administration of normal saline [7]) and use of low-osmolality ICM.

ICM also have a relatively high viscosity, which makes it hard to inject through small catheters and needles. For the same reason, some small vessels will not be shown as the contrast media cannot pass through them or through very tight stenoses.

Another issue with ICM is their elevated cost, especially for LOCM and IOCM, to which one must add the costs of the cures that become necessary in case of adverse effects [5].

1.1.3   Carbon dioxide as a contrast medium

Carbon dioxide (CO_2) can be used as intravascular contrast agent, and it is considered an interesting alternative to traditional ICM.

Due to its unique properties, such as the low viscosity and the lack of allergic reactions and renal toxicity, it has become particularly helpful in patients with compromised renal function or hypersensitivity to iodinated contrast material. This contrast agent is also more advantageous than the traditional ICM from an economical point of view, as medical-grade CO_2 is practically zero-cost. Its use is thus spreading even on patients with no particular risk factors for traditional contrast media.

On the other hand, the use of CO_2 presents some technical difficulties due to its gaseous properties. Furthermore, ICM still represent the gold standard for angiographic procedures, as they generally give better images.

Considering both its advantages and disadvantages, CO_2 is gaining growing attention as a contrast media, not only as a complete replacement of traditional ICM, but for their combined use.

The use of CO_2 gas as an imaging agent dates back to 1914, and it was routinely used in the 1950s and 1960s for the detection of pericardial effusion. In the 1970s it was first used as an intra-arterial contrast agent, but it became much more reliable after 1980, with the advent of DSA.

Properties and potential complications

Unlike most liquid contrast agents, which mix with the blood and fill the lumen, carbon dioxide is a gas that displaces the blood forming bubbles. CO_2 is a negative contrast agent, as it absorbs X-rays to a lesser degree than the surrounding tissues. For this reason CO_2 angiographies look like a negative version of the traditional ones, with white vessels on a darker background.
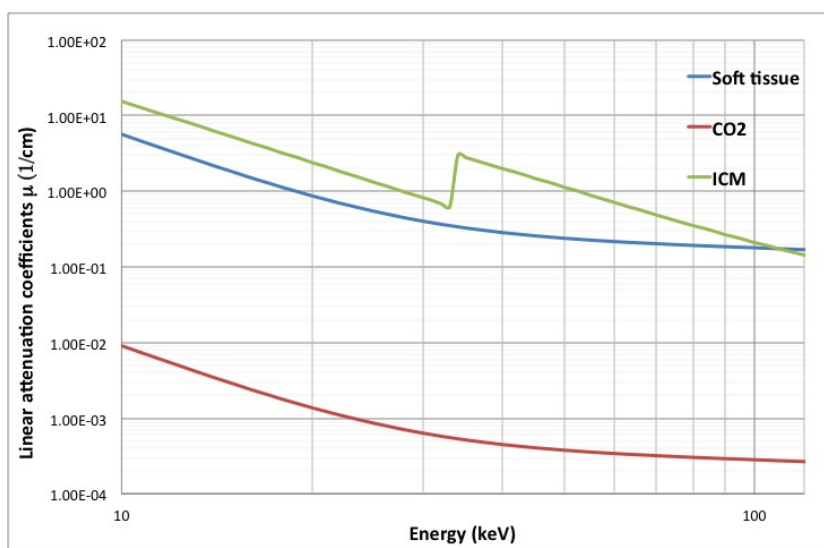
Figure 1.2: Linear attenuation coefficients of ICM, CO_2 and soft tissue.

Figure 1.2 shows the linear attenuation coefficients of traditional ICM, CO_2 and soft tissue (ICRU-44) as functions of the radiation energy. It can be clearly seen that, while iodine has a K-edge at 33 keV, CO_2 has no notable irregularities. The X-ray absorption of CO_2 is roughly $1/10$ of that obtained with diluted iodine and, as it is not highly different from surrounding tissues, it produces less contrast [12].

With the use of enhancement techniques such as DSA, however, it is possible to obtain results with a diagnostic accuracy comparable to ICM in a majority of cases (figure 1.3).

CO_2 is 400 times less viscous than ICM [9]. This characteristic is a great advantage for angiographies not only as it allows the quick injection of large volumes of the gas through very small catheters, but it also allows CO_2 to pass through small vessels, visualise tight stenoses and collaterals, and small bleeding. An example of this power is shown in figure 1.4: during an intervention for the revascularisation of the anterior tibial artery, the
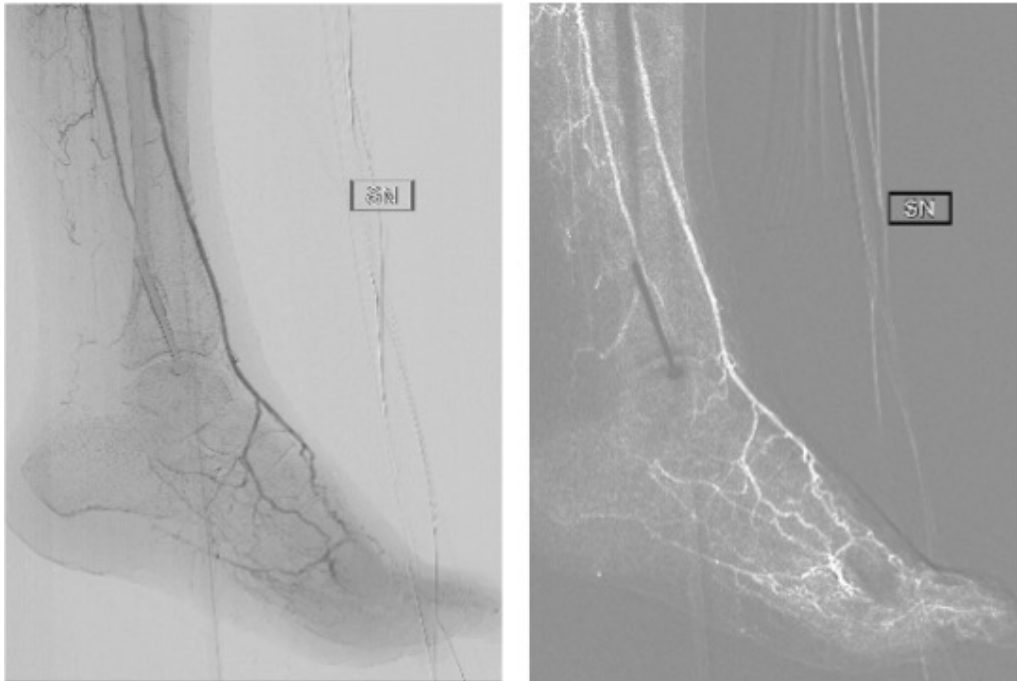
Figure 1.3: Dorsalis pedis artery DSA, with ICM and CO_2 respectively.

radiologist needs morphological informations on the vessels to decide if and where it is possible to insert an angioplasty balloon catheter. In the first image, obtained through traditional ICM angiography, the artery on the right seems blocked: this may lead the radiologist to desist on unclogging that particular vessel. In the second image, on the other hand, the artery is clearly open on the bottom. In fact, thanks to its extremely low viscosity, CO_2 can easily pass through the clogged section of the artery, thus correctly imaging to the rest of the vessel.

When CO_2 is injected in a large vessel it cannot completely displace the blood and, being lighter than blood plasma, it forms bubbles that flow along the anterior part of the vessel. This is not a problem in small vessels, as CO_2 angiography would not significantly underestimate the diameter of a vessel as long as at least 50% of its luminal diameter is filled with the gas (the luminal gas filling is usually greater than 70% in vessel sizes up to 15mm [9]). Nevertheless, an incomplete filling will lead to non-optimal contrast. The gas buoyancy may also cause preferential filling of some branches, based on patient positioning. It is therefore fundamental to carefully choose the patient's position, and eventually to change it as suitable during the procedure.
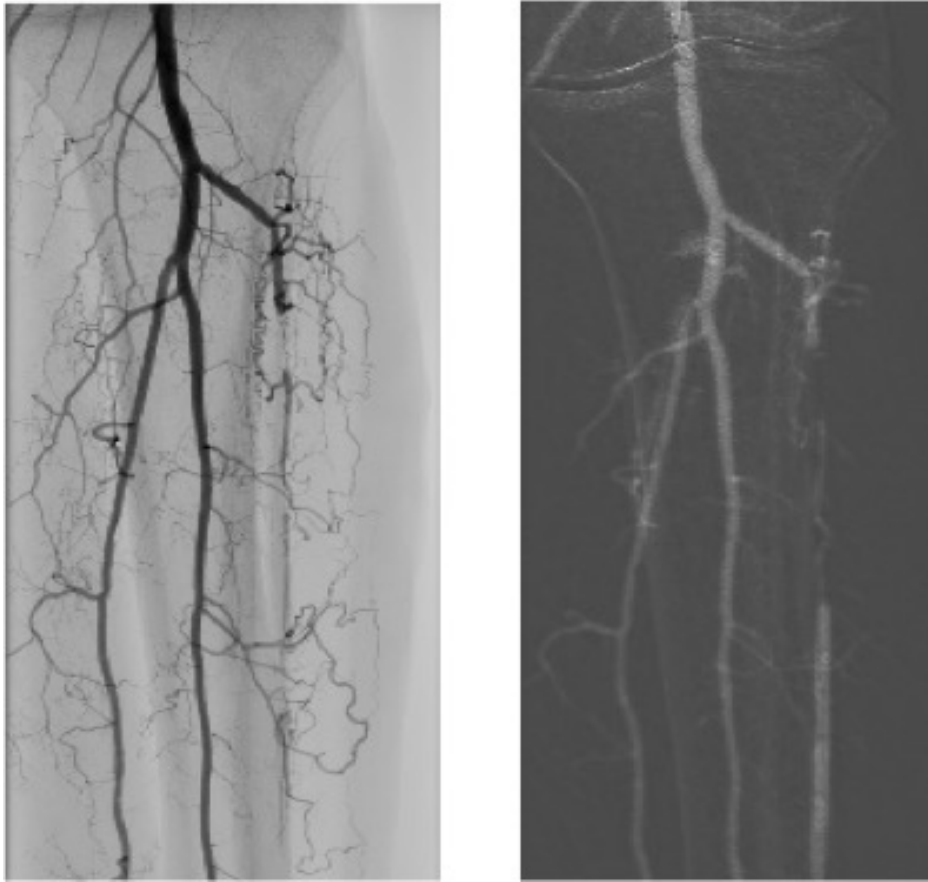
Figure 1.4: Anterior tibial artery revascularisation, with ICM and CO_2.

A great advantage of the use of CO_2 is that it causes no allergic reaction, and experimental and clinical data also indicate that carbon dioxide causes no renal toxicity nor hepatic toxicity. This makes it an ideal alternative to ICM for patients with a history of allergic reactions, but also for patients with diabetes or compromised renal function.
CO_2 is considered safe for intravascular injections because of its high solubility rate (being approximately 20 times more soluble in water than air [9]), hence it does not lead to clinically significant gas embolism.

After the injection, bubbles rapidly flow into the heart and pulmonary artery, and dissolved CO_2 is completely removed by pulmonary expiration. This process usually requires 2-3 minutes, and in general no gas bubble should be seen in the pulmonary artery at 20-30 seconds after the injection.
Thanks to its high tolerance and solubility, the amount of injectable CO_2 is virtually unlimited, as long as the operator allows sufficient time for its
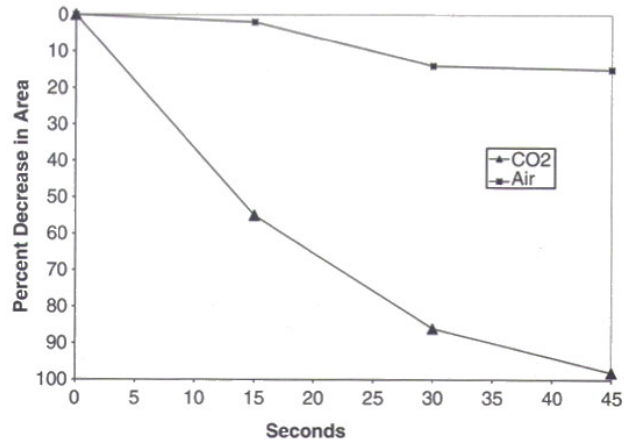
Figure 1.5: Percent area decrease of CO_2 and air bubbles in the right atrium, after intravenous injection of 5cm^3 [9].

clearance (it is considered safe to inject quantities up to 100cc with intervals of minimum 2 minutes between injections).

The use of CO_2 still requires some fundamental precautions.
As studies have indicated its possibile neurotoxicity, CO_2 should never be injected in the cerebral arterial circulation. For safety reasons, arterial studies are generally limited to below the diaphragm.

The delivery of CO_2 in the vascular system is further complicated by its gaseous properties. First of all, CO_2 is a colourless and odourless gas, and as such it cannot be visually distinguished from air. This is one of the most important issues with this technique, as accidental air contamination could cause serious complications such as air embolism.
Taking into consideration its buoyancy, CO_2 is never to be injected in the prone position (to avoid spinal cord ischemia) nor with the patient's head in an elevated position. Important adverse effects are related to the "vapor lock" phenomenon, when the gas is struck and obstructs the normal blood flow. This is usually due to the accidental injection of an eccessive volume of CO_2, and might lead to ischemia or heart failure. In case CO_2 gets trapped it is important to rotate the patient, thus releasing the trapped gas and re-establishing the blood flow.
It should also be noted that CO_2 is compressible during injection and it suddenly expands at the exit of the catheter, resulting in an "explosive delivery". Nevertheless studies have shown that real damage risk for the patient is not due to the gas jet from the catheter but to the local pressure rise, due to the sudden gas input in the elastic vascular chamber [12].

This local increase of pressure might be one of the causes of the transient pain or discomfort that some patients complain after CO_2 injections, along with the temporary acidosis due to the increase of carbonic acid in the blood.

Delivery systems

Considering these technical issues, the choice of a good delivery system is of fundamental importance to reduce the possible risks and allow a better control on the injection, and thus on the final images.

Initially, a *handheld syringe system* was used: a syringe was directly filled from a CO_2 cylinder, employing a gas regulator to reduce the pressure. This technique holds a few important problems, such as the elevated risk of air contamination. Moreover, as there is no control over the injected volume and the injection pressure, this system will result in a highly unpredictable delivery.
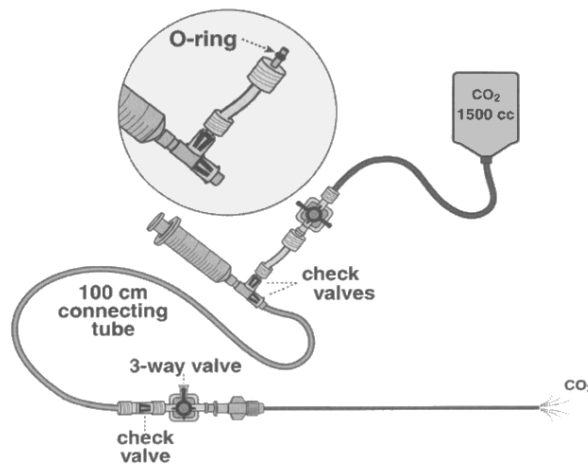
Figure 1.6: Plastic Bag Delivery System [9].

An improvement of this technique was the *plastic bag delivery system* (figure 1.6). A CO_2 cylinder is used to fill a plastic bag that can only contain 1500cc at atmospheric pressure: this prevents the inadverted injection of excessive volumes. The risk of air contamination is averted with the use of multiple one-way check flow valves. This system is quite user-friendly and undoubtedly safer than the handheld syringe, but it still requires a manual injection. Therefore the control of the injection is heavily dependent on the ability of the operator, and errors are possible even with experienced personnel.
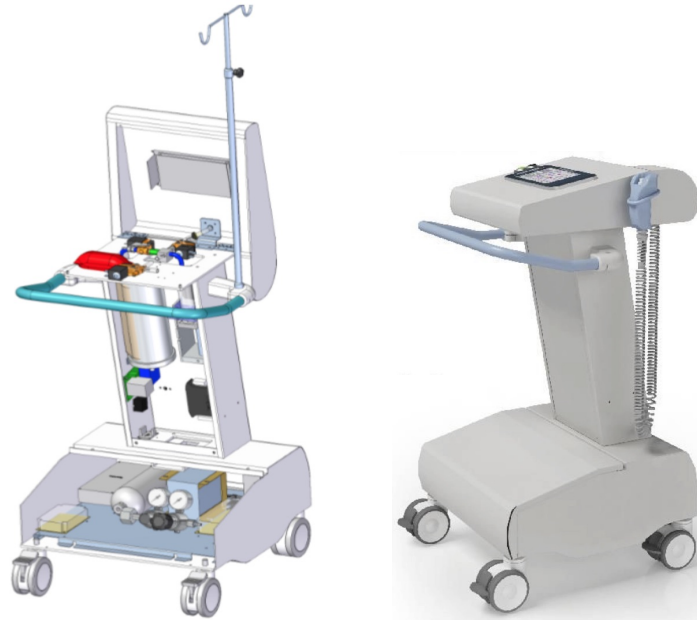
Figure 1.7: "Angiodroid" injector module.

Automatic injectors are quite promising, as they are virtually fail-safe. There is no chance of delivering excessive volumes, injection pressure can be controlled and there is no risk of air contamination.

"Angiodroid" is an automatic CO_2 injector dedicated to diagnostic and interventional angiographic peripheral procedures, produced by BioSpark Srl. This injector allows a precise control over the injection pressure and volume while eliminating any risk of air contamination. The main component of the device is the injector module (figure 1.7).

CO_2 is initially contained in a cylinder, from which it's moved to a 'loading tank' that can hold up to 400 ml of gas. This tank is always kept at positive pressure, thus removing any risk of contamination: even in case of leakage the CO_2 will flow out, rather than the air flowing in. The desired volume of CO_2 is then moved to the 'injection bag', a soft sack that can contain up to 100 ml. This bag is in contact with a 'pressurized tank' which, filled with up to 700 ml of air, can exert an adjustable pressure on the injection bag, thus allowing the regulation of the CO_2 injection pressure. With this delivery system the injection pressure is almost constant, as compared with manual injections (figure 1.8).

Being an automatic system, "Angiodroid" is very user-friendly: the operator can just set the desired CO_2 volume and the pressure of injection, and

the systems automatically delivers the contrast medium. This also reduces the training period for the operators, making CO_2 DSA a more accessible procedure.
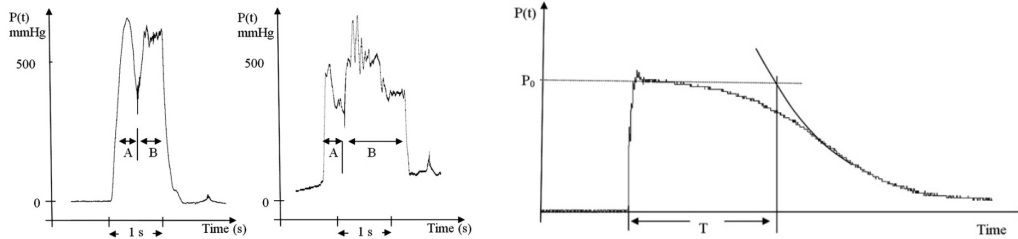
Figure 1.8: Injection pressure as a function of time, for manual injections and with an automatic injector [12]. Manual injections include a phase A of line washing and B of actual CO_2 injection.

1.2   Radiological systems

Interventional radiology procedures are usually performed in angiographic suites equipped with C-arm systems called fluoroscopes. This radiological system comprises a high power generator, an X-ray tube, an image receptor and an automatic exposure control system. The radiological apparatus can be set in different ways, but the most common configuration is with the X-ray tube located under the patient table, and the imaging equipment above the patient. Fluoroscopes can be both floor-mounted or mobile. Mobile fluoroscopes are useful when they need to be moved between locations, but they are generally less powerful (about 15kW instead of circa 100kW).

These radiological systems have multiple operating modes, to adapt their function to the operative diagnostic and therapeutic needs, and can perform both fluoroscopy and radiography.

Fluoroscopy is used to monitor the introduction of catheters and guides through the vascular system to the desired location. For this purpose, a limited photon flow is sufficient, so the X-ray tube operates in a continuous mode with a current of a few mA (usually up to 5 mA).

When a detailed description of vascular chambers is needed, the photon flow is increased by rising tube current, and the emission changes from continuous to impulsive. This is the true angiographic phase, which uses currents up to 1000 mA and frame rates up to 50 fps with frame lengths varying from a few to about 40 ms. A pulsed emission may also be applied to fluoroscopy:

the introduction of pulsed fluoroscopy reduces patient dose while improving image quality, as it avoids unnecessary exposition while allowing the use of greater dose rates.

Due to the complexity and length of the procedures, which can easily take up to more than one hour, interventional suites need to be equipped with powerful generators and X-ray tubes with valid cooling systems.

1.2.1   X-ray generator

The X-ray generator is the component that provides all the electrical power sources and signals required for operating the X-ray tube, and controls the operational conditions of X ray production. Its essential components are a filament heating circuit to determine anode current, a high voltage supply to accelerate the anode current electrons, a motor drive circuit for rotating the anode and an operational control to regulate the voltage and currents.

The filament circuit heats the X-ray cathode filament according to the set tube current. Even when not emitting, the filament is permanently preheated to a temperature at which thermionic emission is negligible, in order to minimize thermal stress and increase its durability. The filament also presents a thermal inertia, which limits the speed of changes in tube current. To allow a fast switching of the tube current (e.g. when pulsed emission is required) some tubes use a negatively biased grid positioned near the filament to shut out the flow of electrons ("grid-switched" X-ray tubes).

A fundamental function of the X-ray generator is to provide a high voltage to the X-ray tube. As the AC line voltage available in hospitals (380V three phase) is much lower than the voltage required for X-ray production (40 to 150 kV), a voltage elevation circuit is necessary.

Modern voltage elevators use a tree step solution:

- A first circuit transforms the AC line power into DC power;

- A second circuit transforms the DC voltage into a high frequency alternating PWM signal;

- A transformer receives the high frequency PWM signal and produces a high voltage signal, which is then rectified by diodes and applied to the tube.

The voltage is usually supplied symmetrically to the tube: for example a potential difference of 120 kV is achieved by applying -60 kV to the cathode
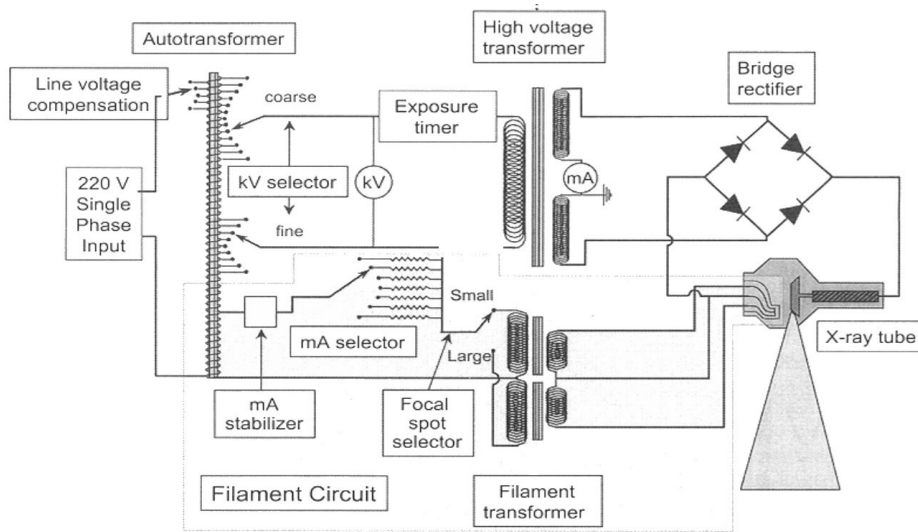
Figure 1.9: Schematic view of an X-ray generator [15].

and +60 kV to the anode. During angiography or pulsed fluoroscopy the X-ray emission is controlled by rapid tube voltage changes or by a tube grid interruption system. When controlling the emission by tube voltage, it is important to reach the desired voltage in the shortest possible time. This time is limited by the electronic circuits and by the capacitance of the high voltage cables, resulting in a modified HV pulse with non-null rise time and some tailing, which not only impairs the production of short pulses, but also changes the emitted X-ray spectrum.

An operator console allows the selection of X-ray tube parameters, such as kVp, mA, exposure time and, on some generators, the focal spot size. For fluoroscopic systems this selection is usually piloted by the automatic exposure control system.

1.2.2 X-ray tube

The principal components of an X-ray tube are a cathode, composed of one or more tungsten filaments in a focusing cup, and an anode. Both are contained inside a tube envelope to maintain an interior vacuum and, together with a motor for anode rotation, they are contained inside a metal housing (figure 1.10).

The current, passing in the helical filament of the cathode, controls the thermionic emission of electrons, changing the intensity of the X-ray beam. X-ray tubes for diagnostic images typically have two filaments of different
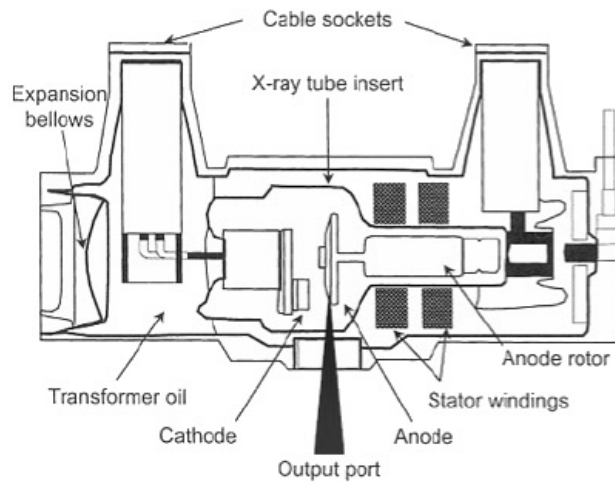
Figure 1.10: Schematic view of an X-ray tube [15].

sizes, as their lengths determine the focal size. A smaller filament means a smaller focal spot, and subsequently more detailed images. On the other hand, a longer filament allows a better heat dispersion on the anode, thus allowing to work with higher powers.

Most X-ray tubes have a rotating anode, commonly made of tungsten because of its high atomic number (Z=74) and high fusion point (3422°C). Molybdemun (Z=48) and rhodium (Z=45) anodes are also used for specific applications, such as mammography.

The area of the anode hit by the electrons should be as large as possible, in order to keep the power density within acceptable limits. The anode is angled to balance this need with the goal of obtaining a small focal spot size, for the line focus principle: the "effective" focal spot length is much smaller than its "true" length, as shown in figure 1.11, and the corresponding geometrical relation is:

$$\text{"effective" focal length} = \text{"true" focal length} \cdot sin\theta$$

where θ is the anode angle.

These elements are enclosed in a glass envelope under a high vacuum. This is then contained within a X-ray tube housing filled with oil, which supports, insulates, and protects the X-ray tube insert from the environment. The housing also contains lead shields to attenuate the X-ray that are emitted in directions other than the desired one.
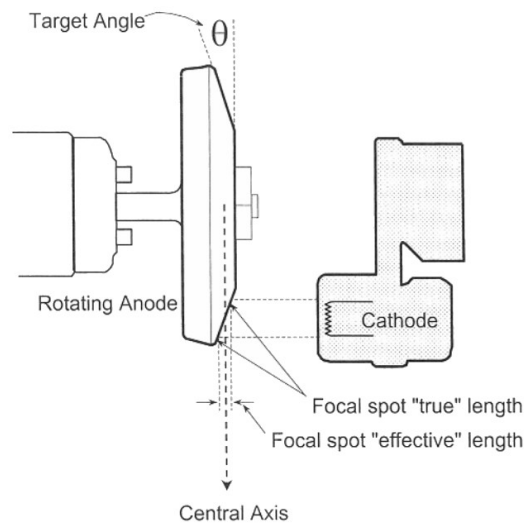
Figure 1.11: Line focus principle [15].

X-ray beam filtering changes the shape of the spectrum. The X-ray beam is subject to some filtration caused by the tube itself, such as the one due to the glass or metal insert at the x-ray tube port. Besides this inherent filtration, an added filtration is usually included in order to selectively remove some components of the spectra. Low energy components are usually eliminated, as they are not useful for image formation but just increase the patient dose.

Different emission parameters further change the beam characteristics. Radiation quality refers to the beam's penetrating ability. As it is tied to the spectrum shape, it can be changed with tube voltage, which determines the maximum energy in the spectrum. X-ray beam quality is often expressed by its half-value thickness (HVL) in mmAl. The beam intensity depends on the number of electrons emitted from the cathode and their energy, thus it is influenced by tube voltage, anode current and exposure time (X-ray beam intensity is roughly $I \propto kVp^2 \cdot mAs$ [15]).

The energy incident on the anode causes a buildup of heat which, if not efficiently dissipated, might cause anode rupture. The nominal anode input power is $P = kV \times mA$, considering the tube voltage and the anode current. Heat dissipation occurs by irradiation, following Boltzmann's law. Each X-ray tube has a graph with its anode heating and cooling curves for different applied powers, as they can greatly vary from tube to tube. For

example, comparing two different tubes (figure 1.12 and figure 1.13) we can see that the stored energy is on a completely different scale (maximum 225 kJ versus more than 2500 kJ).

Along with this graph, each equipment should be provided with two graphs of the heating and cooling curves of the X-ray tube assembly, a "passive" one and and "active" one in case a cooling system in function.
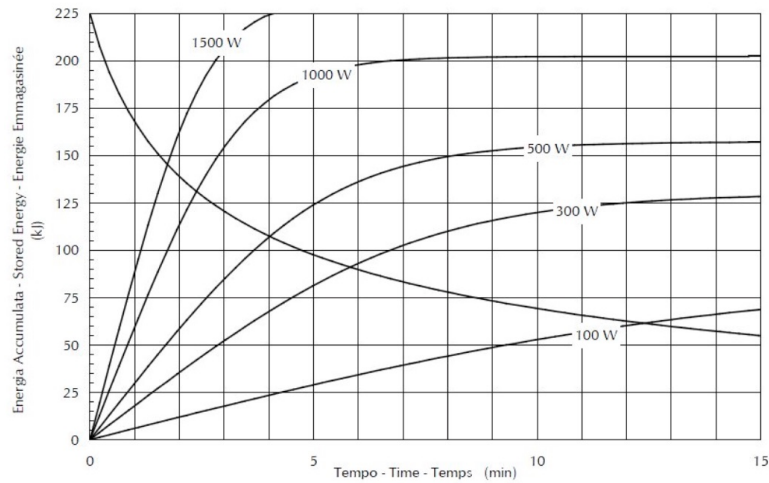
Figure 1.12: Anode heating and cooling curves for RTM 70 H [23].
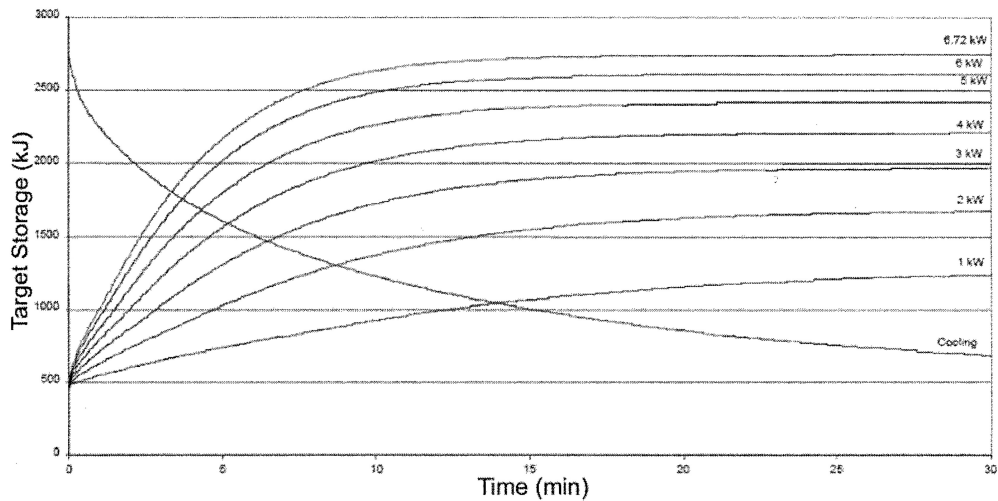
Figure 1.13: Anode heating and cooling curves for Performix 160 A [24].

1.2.3   Image detectors

X-ray image intensifiers

The introduction of X-ray image intensifiers (II) in the early 1950s revolutionized the use of fluoroscopy in clinical diagnosis, making it possible to obtain continuous X-ray imaging at reasonable exposure.

Image intensifiers are vacuum tube devices that, with a three-stage conversion and amplification process (figure 1.14), can convert low intensity X-ray photon fluence exiting the patient into a high fluence of visible photons. The most commonly used scintillator is thallium-doped cesium iodide (CsI:Tl), which is usually grown as needle-shaped crystals with 5-10 μm in diameter. This structure acts as a light-guide, reducing the scattering of the light during its path to the photodiode, thus increasing spatial resolution. X-ray photons strike the CsI input phosphor, where they are absorbed and produce a large number of visible light photons. A photocathode produces a corresponding number of electrons, which are accelerated and focused as to impact on the output phosphor. This collision results in the emission of light photons that can be recorded by a video camera, and the resulting image accurately represents the X-ray distribution incident at the input window.
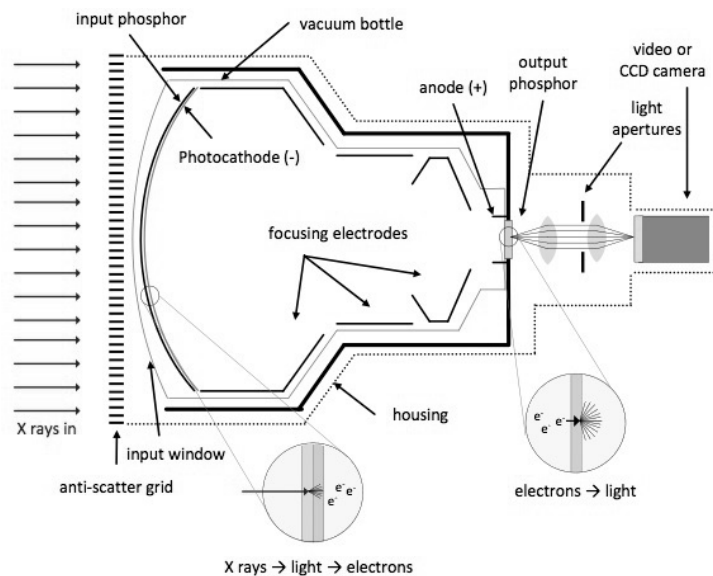
Figure 1.14: Schematic view of an image intensifier [14].

This systems holds many potential sources of error. The input phosphor needs to be curved to withstand external atmospheric pressure, but mapping a curved input surface onto a flat output surface leads to a spatial distortion

at the periphery of the image (pin-cushion distortion). Furthermore, electrostatic and magnetic focusing gradients may interact with magnetic fields, causing transient spatial 'S' distortions. The images also present vignetting caused by light scattering from the output phosphor. This also causes veiling glare, which reduces the overall image contrast. Spatial resolution is determined by the video camera system and the magnification mode of the field of view. Even though the II has a linear light intensity response over a very wide range of incident exposures, this is not true for the video cameras, and some of the image information content is lost by saturation or threshold of the signals.

Flat panel detectors

Flat panel detectors (FD) were first introduced in the late 1990s, and had a widespread diffusion due to their ability to cover the various requirements of different applications, ranging from general radiography to mammography and fluoroscopy [17]. In particular, in interventional radiology, they have almost completely substituted the image intensifier systems.

The central component of flat-panel detectors is an active matrix of hydrogenated amorphous silicon (a-Si:H), with a pixel structure of photodiodes and thin-film transistors (TFT). The conversion process of X-ray radiation into electric charge can be of two different types: an indirect conversion process, in which the X-ray radiation is first converted into light, which then creates electric charge, and a direct conversion of X-ray into electrical charge.
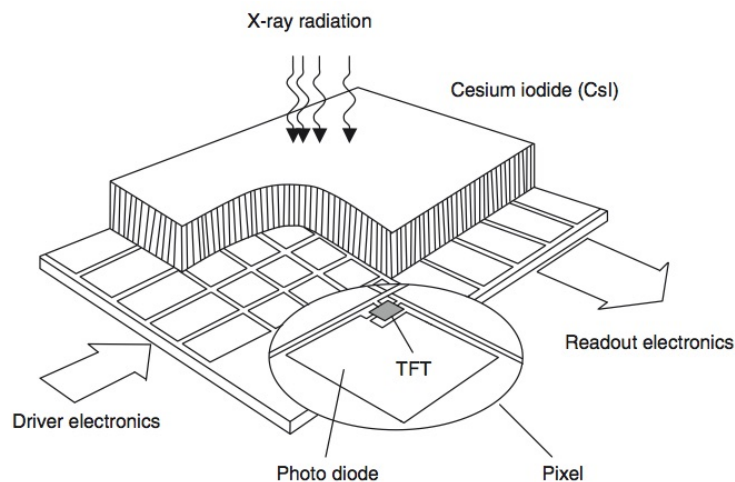
Figure 1.15: Schematic view of an indirect converting flat detector based on CsI and an amorphous silicon active readout matrix [17].

The most widely used type of conversion is the indirect process, with CsI as scintillator material (figure 1.15). The X-ray quantum is absorbed creating a high-energy electron via photo absorption. This electron looses energy in the scintillator material creating a large number of electron-hole pairs, which in turn recombine to produce photons in the visible range. This light is then converted to electric charge when it hits the photodiode, which is designed to reach a high quantum efficiency in the green part of the visible spectrum to match the spectrum of the scintillation light. After each exposition, the pixel circuit performs a row by row readout, and the signal is fed to an analog-to-digital converter.

Flat panel detectors possess several advantages over image intensifiers, like better image uniformity, no veiling glare or vignetting, and small, thin physical size. Geometric distorsion is not an issue, as FDs are not influenced by magnetic fields and there are no curved surfaces involved. A great advantage of flat panels is their high degree of linearity for a wider dose range than IIs. On the other hand, while this holds true for most applications (especially for high-exposure applications like DSA), FDs are less efficient for low exposure levels due to the increased contribution of electrical noise. Figure 1.16 shows that the dynamic range of an image intensifier fluoroscopy system is smaller than that of a FPD system. Other issues with FDs are the lower spatial resolution, which is determined by the actual size of the detector element, and the higher costs.
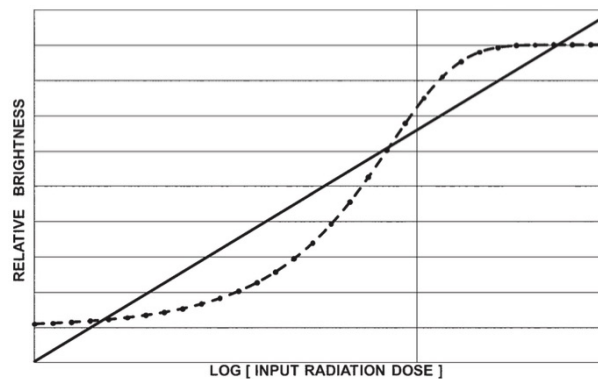
Figure 1.16: Graph plots the dynamic ranges of an image intensifier (dashed line) and FPD (solid line) fluoroscopy system [19].

1.2.4   Automatic exposure control

Radiological suites include an automatic exposure control (AEC) system to automatically adjust the irradiation parameters to deliver a constant signal intensity in response to different patient thicknesses, X ray tube energies, focus to detector distances and other technical factors.

Usually, AEC systems sense the light output using a sensor (such as a photodiode or a photomultiplier) or the detected image itself, and this signal is used in a feedback circuit to the X-ray generator to regulate its parameters. For fluoroscopic systems, AEC changes tube voltage and anode current. In some pulsed-fluoroscopy systems, AEC might also regulate pulse widths. The selection of the parameters follows predetermined curves that are stored in the generator and which usually allows for some choices, including a standard curve, low dose curve and high contrast curve (figure 1.17).
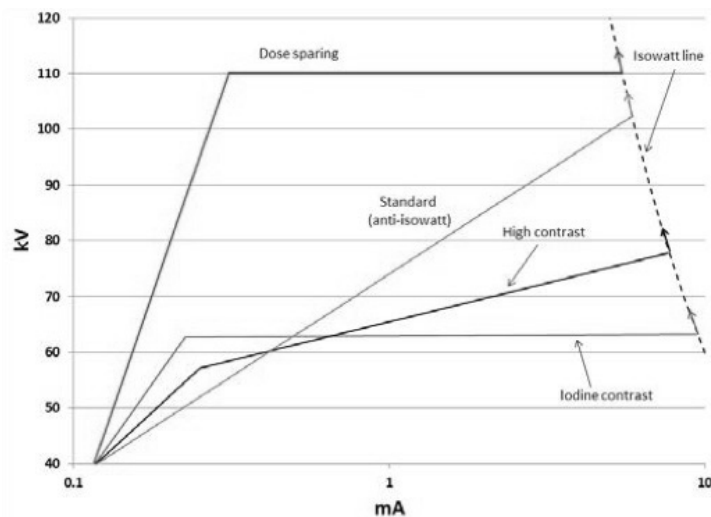
Figure 1.17: An example of typical control curves for an AEC system [14].

1.3 Radioprotection in medical exposures

The International Commission on Radiological Protection (ICRP) is an independent international organisation founded in 1928 to provide guidance on protection against ionising radiation. Legislations, guidelines and programmes on radiation protection are based on ICRP's reports and recommendations. The latest recommendations are contained in "The 2007 Recommendations of the International Commission on Radiological Protection" (ICRP Publication 103 [20]), which are un update of the 1990 version (ICRP Publication 60).

Radiological protection is based on three principles: the principle of justification, the principle of optimisation of protection and the principle of application of dose limits. The first two apply in all situations, while the latter only applies in cases of planned exposure.

- **The principle of justification**: Any decision that alters the radiation exposure situation should do more good than harm.

- **The principle of optimisation of protection**: The likelihood of incurring exposures, the number of people exposed, and the magnitude of their individual doses should all be kept as low as reasonably achievable, taking into account economic and societal factors.

- **The principle of application of dose limits**: The total dose to any individual from regulated sources in planned exposure situations other than medical exposure of patients should not exceed the appropriate limits recommended by the Commission.

The document distinguishes three types of programmed exposures: occupational exposures, public exposures, and medical exposures of patients. The latter mainly indicates exposures to patients undergoing diagnostic examinations, interventional procedures, or radiation therapy.
Medical exposure has to be handled with a different approach compared to the others cases, because it is intentional and directly benefits the patient.

For the principle of justification it is important to make an accurate evaluation of every medical procedure involving radiation exposure. As it is now generally accepted that the use of radiation in medicine does more good than harm to the patients, the evaluations focus on determining whether a specific radiological procedure will usually improve the diagnosis or treatment. It is then necessary to make a risk-benefit evaluation of the procedure for

individual patients (e.g. checking that the proposed procedure is the most suitable method, or that the required information is not already available).

After a procedure has been appraised as justified, it is the turn of its optimisation. It is important to remember that, especially in the medical field, *optimisation of protection is not minimisation of dose*, hence the best option is not necessarily the one with the lowest dose.
In the case of radiation therapy, an optimised procedure delivers the prescribed dose to the tumour while protecting as much as possible the healthy tissues outside the target volume. In diagnostic and interventional procedures, optimisation involves keeping doses as low as reasonably achievable without defeating the purpose of the procedure.

ICRP does not recommend the application of dose limits for medical exposures, as they may do more harm than good by reducing the effectiveness of the treatment or diagnosis. Instead of limits, the document suggests the assessment of *diagnostic reference levels* as a term of comparison to indicate whether the levels of patient dose are unusually high or low for that procedure. In such cases, it is necessary to re-evaluate the optimisation of the procedure.

1.3.1   Dosimetric quantities

The fundamental physical quantity in radiation biology, clinical radiology, and radiological protection is the *absorbed dose*, D, defined as the mean energy imparted to a unitary mass by ionising radiation.

$$D = \frac{d\epsilon_{ads}}{dm}$$

The absorbed dose is not the same as the *kerma*, K, which is defined as the mean energy transferred from indirectly ionizing radiation to charged particles in the mass dm.

$$K = \frac{d\epsilon_{tr}}{dm}$$

As kerma may be defined in any material, it is important to declare the material considered (e.g. air kerma).
The SI unit for both absorbed dose and kerma is the gray ($1\ Gy = 1\ J \cdot kg^{-1}$), but the two quantities are not equivalent as the energy transfer from the primary photon does not happen in the same place of the energy deposition in the material.

Kerma and absorbed dose have the same value only in condition of electronic equilibrium, in which the charged particles that are released in a volume dV and the ones that leave the volume are balanced. In case of unattenuated photon beams this condition is met after a certain depth, called build up region, of the order of the charged particle range in the material. In a more realistic situation the attenuation of the photon beam cannot be neglected and, after the build up region, we reach a state of transient electronic equilibrium in which both kerma and absorbed dose decrease with depth. For this approximate electronic equilibrium to subsist, the X-ray attenuation must be very small: for water and soft tissues, this is certainly the case for primary photons with energies from 0.1 to 0.5 MeV, and it increases exceeding 5% at 3 MeV [13].

As the absorbed dose cannot be measured, it is usually calculated from other quantities. In case of equilibrium between kerma and absorbed dose:

$$D = K(1 - g)$$

where g is the fraction of energy that is lost to bremsstrahlung.
In practice, the absorbed dose values are averaged over tissue volumes, usually over the mass of a specified organ or tissue.

The *equivalent dose* is a quantity that takes in consideration the biological effectiveness of the type and energy of radiation:

$$H_T = \sum_R w_R D_{T,R}$$

where w_R is the radiation weighting factor for radiation R, as determined ICRP on the basis of experimental data.

The *effective dose* is a quantity that represents the risk of stocastic effects, and is defined as a weighted sum of the equivalent doses of the various tissues.

$$E = \sum_T w_T H_T = \sum_T w_T \sum_R w_R D_{T,R}$$

where w_T is the tissue weighting factor for tissue T. These factors represent the contributions of individual organs and tissues to the overall radiation detriment from stochastic effects as determined by ICRP on the basis of epidemiological studies, and they are $\sum w_T = 1$. The SI unit for both equivalent dose and effective dose is the sievert ($1 \ Sv = 1 \ J \cdot kg^{-1}$).

For what concerns medical exposures, the assessment of patients' doses is of fundamental importance not only for risk-benefit evaluations, but also in order to understand the factors that affect the exposure and to devise effective techniques for its reduction.

In many cases patient dose is described using the *entrance surface dose* (ESD), defined as the absorbed dose measured on the patient's skin at the center of the X-ray beam, or in terms of *incident air kerma*, without the contribution of backscattered radiation.

Another common quantity is the *dose area product* (DAP), which is widely used because it is correlatable to the absorbed dose and it can be easily measured with a DAP chamber without interfering with the patient or the procedure. DAP is usually expressed in $mGy \cdot cm^2$ and is defined as the integral of the absorbed dose over the area of the X-ray beam in a plane perpendicular to the beam axis:

$$DAP = \int_A D(x,y)dxdy$$

In the approximation that the absorbed dose does not vary across the field, this is equal to the product of the absorbed dose and the field area [14].
It is very useful thanks to its property of being approximately independent of the distance from the source, when interactions in air and extrafocal radiation can be neglected, as the dose decreases with the square of the distance while the field area increases with the square of the distance (figure 1.18).
Exploiting this property the DAP chamber is positioned at the exit of the X-ray tube to encompass the whole radiation field, and the value measured in that point should be the same as the value at the entrance of the patient.

distance	50 cm	100 cm	200 cm
dose	4 mGy	1 mGy	0.25 mGy
area	25 cm^2	100 cm^2	400 cm^2
DAP	100 mGy·cm^2	100 mGy·cm^2	100 mGy·cm^2
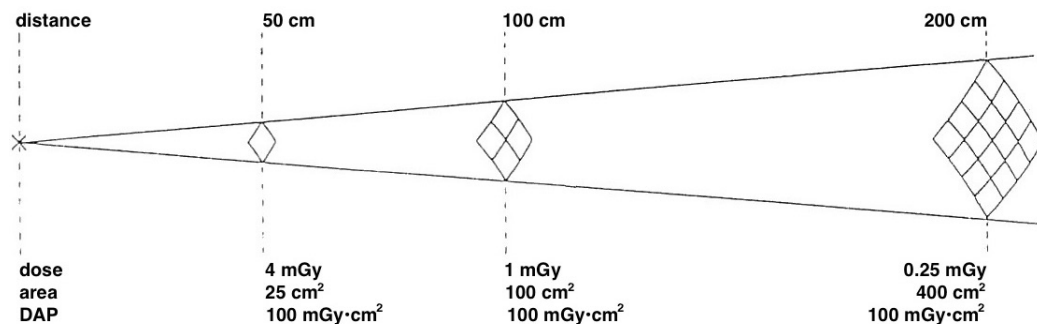
Figure 1.18: Dose area product is independent of distance.

These quantities are adequate where the X-ray exposure conditions are constant, for example for quality control of equipment.

However this is not sufficient for the comparison or the assessment of patients' doses if the irradiation conditions (the size of the patient, the radiation quality, the exposed body-part, or other factors) are changed.
For some purposes, the risk of stochastic harm from ionising radiation can be simply reported with the *effective dose*. However its assessment and interpretation is problematic when the exposure is partial or very heterogeneous, which is the case of most medical procedures, hence it is preferable to evaluate the risks for individual organs or tissues using the *mean absorbed doses* or *equivalent doses* [20].

One of the main issues with both organ doses and the effective dose is that they cannot be measured directly in patients undergoing X-ray examinations. It is possible to obtain experimental measurements using physical phantoms, but the process can be laborious and time consuming. Hence, it is common to calculate these quantities, generally using the Monte Carlo method. The values obtained are reasonably accurate, as the physical interactions between radiation and matter are sufficiently well-known, and the accuracy of the calculation is limited mainly by the accuracy of the anatomical model used to describe the patient and by the characterisation of the applied radiation field.

1.3.2   Radioprotection for IR procedures

Interventional radiology procedures, such as angiographies, are characterised by high level of doses to both patient and medical staff. This is due to the long fluoroscopy time and the large number of radiographic frames per examination. In addition to the increased likelihood of stochastic effects, particularly long procedures might cause deterministic radiation injuries.

The planning of such procedures should follow a guideline for the radiation dose management, such as the one proposed by the Society of Interventional Radiology [22]. Preprocedural preparations should include individual training of the operators, periodical quality assessment of the equipment and careful procedure planning. During the procedure, in accordance with the acting regulations, the operators should constantly monitor the radiation dose through quantities such as DAP and fluoroscopy time. In any case, all the possible dose minimization techniques should be put in action. After the procedure, the estimated patient dose or the measured dose values should be recorded in the patient's medical record. Patients that have received particularly large doses of radiation should be subjected to additional clinical follow-ups.

Materials and methods

2.1 Experimental setup

To take some preliminary measures we used an X-ray tube, the IAE RTM 70 H, which is placed in a bunker at the Centre of Medical Physics of the Bologna University Hospital Authority St.Orsola-Malpighi Polyclinic (figure 3.1).

Manufacturer:	**IAE**
Name:	**RTM 70 H**
Power:	25 kW
Voltage range:	40 ÷ 130 kV
Current range:	0.5 ÷ 140 mA
Focal spot size:	0.3/0.6 mm
Anode angle:	10°
Total filtration:	1.5 mmAl

Table 2.1: Technical data of IAE RTM 70 H.

2.2 Fluoroscopy suites

To study the different irradiation parameters applied by different equipment we worked on 3 different fluoroscopy suites from different manufacturers, all in use at the the St.Orsola-Malpighi Polyclinic.

2.2.1   Ziehm Vision RFD

The first fluoroscopic equipment we considered is a Ziehm Vision RFD mobile fluoroscope. As it is wheel-mounted, it can be easily moved from room to room, but it is less powerful than the other considered suites.

Manufacturer:	**Ziehm**
Name:	**Vision RFD**
Generator:	VISION R-200
Power:	20 kW
Voltage range:	$40 \div 120$ kV
Current range:	$0.5 \div 140$ mA
Tube insert:	RAD 15
Focal spot size:	0.3/0.6 mm
Anode angle:	10°
Total filtration:	5 mmAl
Image detector:	PaxScan 3030
Detector type:	flat panel
Detector size:	30×30 cm

Table 2.2: Technical data of Ziehm Vision RFD.

Figure 2.1: Ziehm Vision RFD.

2.2.2 Siemens ANGIOSTAR

Siemens ANGIOSTAR is a floor-mounted fluoroscope that comes with an image intensifier as image detector. This equipment does not have a CO_2-specific program, so we studied its behaviour for the traditional peripheral DSA protocol.

Manufacturer:	**Siemens**
Name:	**Angiostar**
Generator:	POLYDOROS IS
Power:	100 kW
Focal spot size:	0.3/0.6/1 mm
Anode angle:	12°
Total filtration:	8 mmAl
Image detector:	Sirecon 40-4 HD
Detector type:	image intensifier
Detector size:	40 × 28 cm

Table 2.3: Technical data of Siemens Angiostar.

Figure 2.2: Siemens ANGIOSTAR.

2.2.3   GE Innova IGS

GE Innova IGS is a powerful angiographic system, with a powerful generator and a flat panel image detector. Its anode heating and cooling curves are shown in figure 1.13.

Manufacturer:	**GE**
Name	**IGS Innova**
Generator	JEDI 100
Power	100 kW
Voltage range	$40 \div 150$ kV
Current range	$10 \div 1000$ mA
Tube insert	Performix 160 A
Focal spot size	0.3/0.6/1 mm
Anode angle	11°
Total filtration	1.8mmAl+0.2mmCu
Detector type	flat panel
Detector size	31×31 cm

Table 2.4: Technical data of GE Innova IGS.
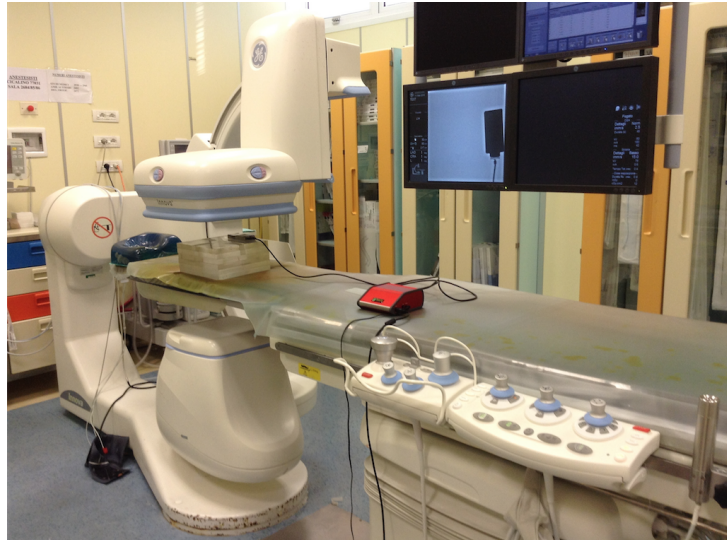
Figure 2.3: GE Innova IGS 530.

Comparison chart

This is a simple chart for the comparison of the three fluoroscopy suites:

Manufacturer:	**Ziehm**	**Siemens**	**GE**
Name:	Vision RFD	Angiostar	Innova IGS
Power:	20 kW	100 kW	100 kW
Focal spot size:	0.3/0.6 mm	0.3/0.6/1 mm	0.3/0.6/1 mm
Anode angle:	10°	12°	11°
Total filtration:	5mmAl	8mmAl	1.8mmAl+0.2mmCu
Image detector:	flat panel	image intensifier	flat panel
Detector size:	30 × 30 cm	40 × 28 cm	31 × 31 cm

Table 2.5: Comparison chart for the considered fluoroscopes.

2.3   Barracuda

Figure 2.4: Barracuda data processing cabinet and MPD.

"Barracuda" by RTI Electronics is an extremely versatile X-ray multimeter that can be used as a quality assurance system. It is a modular instrument whose main parts are a data processing cabinet, a Multi-Purpose Detector (MPD) and a computer with the oRTIgo software. The MPD is a universal semiconductor detector for all types of X-ray systems, and can measure tube voltage, exposure time, dose, dose rate, dose/pulse and pulse rate, total filtration, quick HVL estimation, kVp waveform and dose rate waveform.

Table 2.6 lists the MPD measuring ranges and inaccuracies, as stated on its manual [25].

	Range	Inaccuracy
kVp:	35 - $155kV$	$\pm1.5\%$
Irradiation time:	$0.1ms$ - $2000s$	$\pm1\%$ or $\pm0.5ms$
Dose rate:	$0.2\mu Gy/s$ - $1000Gy$	$\pm5\%$ or $\pm0.02\mu Gy/s$
Estimated HVL:	1.2 - $14mmAl$	$\pm10\%$ or $\pm0.2mm$

Table 2.6: MPD measuring ranges and inaccuracies.

When recording waveforms the sampling rate is inversely proportional to the acquisition time, as the memory size is limited. The recording time can

span from 320 ms (with a sampling rate of 2000 times per second) to 41 s (with 16 acquisitions per second). The recording can be triggered manually or by the system, usually with the start of the irradiation. When trigged by the system, the waveforms will be stored from the start of the exposure to the maximum recording time stated below, or until the end of the exposure if the exposure is finished before the memory is full.

2.4 SpekCalc

The X-ray spectrum and beam quality are fundamental parameters for studying the dosimetric properties of X-ray beams in medical physics. Direct measures of the true spectral photon fluence require a spectrometer and careful set-up planning. For most uses, therefore, X-ray prediction models are usually applied.

SpekCalc is a software program for the calculation of X-ray spectra from tungsten anode X-ray tubes. It can simulate a wide range of tube voltages (40-300 kVp) and anode angles (6-30°), with filters of seven possible materials (air, water, Be, Al, Cu, Sn and W). In addition to the simulated spectrum, the GUI also shows the 1st and 2nd HVL in both mmAl and mmCu, the mean energy of the spectrum, the effective energy for Al and Cu and the estimated bremsstrahlung and characteristic contributions to the tube output.

Its theoretical approach was developed by Gavin Poludniowski and Phil Evans at The Institute of Cancer Research of London [28, 29]. This model combines numerically pre-calculated electron distributions with deterministic equations, based on theoretical results for the bremsstrahlung cross sections. Despite its limitation, due to some simplifying assumptions, this program represents a valid alternative to a full Monte Carlo treatment of the problem [30], and its predictions are comparable to experimental measures [31].

CHAPTER 3

Results

3.1 Evaluation of X-ray attenuation with PMMA

Firstly, we evaluated the attenuation of X-ray beams with different thicknesses of PMMA, which is the material we chose for the phantom in the subsequent measures.

Using the X-ray tube RTM 70 H we recreated five standard RQR beams, based on the IEC normative 61267:2005-11 [27]. RQR beams represent a standard for radiation beams emerging from the X-ray tube, and table 3.1 indicates the tabulated values for radiation qualities of the considered beams.

Radiation quality	Tube voltage (kV)	HVL (mmAl)
RQR2	40	1.42
RQR4	60	2.19
RQR6	80	3.01
RQR8	100	3.97
RQR9	120	5.00

Table 3.1: RQR beam qualities as tabulated in the IEC normative [27].

The required beams were recreated choosing an appropriate added aluminium filtration for each tube voltage, and evaluating the resulting experimental beams using the Barracuda MPD dosimeter. Table 3.2 shows the

obtained values, with their errors due to the Barracuda reading inaccuracy, which are in good agreement with the required values.

	Voltage(kV)	HVL(mmAl)	Added filter(mmAl)
RQR2	(40.5 ± 0.6)	(1.38 ± 0.14)	1.8
RQR4	(60.7 ± 0.9)	(2.2 ± 0.2)	1.5
RQR6	(79.8 ± 1.2)	(3.1 ± 0.3)	1.8
RQR8	(101.6 ± 1.5)	(4.0 ± 0.4)	2.2
RQR9	(121.1 ± 1.8)	(5.1 ± 0.5)	2.3

Table 3.2: Experimental beam qualities measured with the Barracuda dosimeter, and their respective added filtration.

Figure 3.1: The considered setup, composed of the RTM 70 H X-ray tube, PMMA slabs and the Barracuda MPT dosimeter, secured on a flat panel.

These RQR beams were then attenuated with an increasing number of PMMA slabs, with a depth of 2 cm each, to evaluate their attenuation. This setup is shown in figure 3.1. Figure 3.2 shows for each beam the attenuation of the dose rate, measured with the Barracuda dosimeter, as function of the

thickness of the inserted PMMA slabs. The results cannot be fitted with an exponential interpolation, as the beams are not monoenergetic.
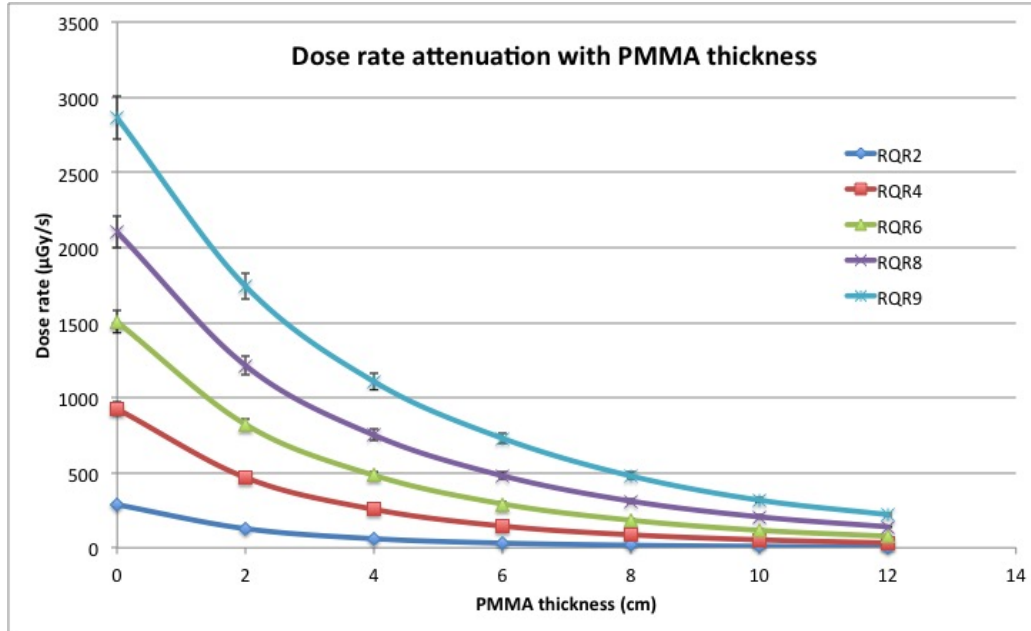
Figure 3.2: Dose rate attenuation with increasing PMMA thickness.

From the obtained data, it is possible to calculate the thickness of PMMA necessary to produce beams with the same radiation quality of RQA beams, which are the standard for attenuated beams as tabulated in the IEC normative [27]. The HVL of each beam increases linearly with the thickness of the PMMA phantom. With a linear interpolation, we can easily extract the thickness of PMMA that gives a beam with a certain HVL.

Radiation quality	HVL (mmAl)	Required PMMA (cm)
RQA2	2.2	8.6
RQA4	5.4	26.6
RQA6	8.2	33.4
RQA8	10.1	36.2
RQA9	11.6	41.4

Table 3.3: Thickness of PMMA required to produce RQA beams.

3.2   Measures on radiological systems

Radiological suites from different firms implement different programs, and as such they might operate differently for the same situation. We are interested in investigating how different equipments perform fluoroscopy with DSA, in both traditional and CO_2-specific program. The inspected equipments operate on pulsed-mode, allowing the operator to choose a determinate pulse rate (in frames per second).

To analyze the behavior of different radiological suites, we recreated the same set-up on all the apparatus: in stead of the patient we put a phantom made of 12 cm of PMMA slabs, positioning the dosimeter on its side. We acquired the dose rate waveforms with the Barracuda MPD dosimeter, set to a maximum recording time of 3 seconds after the beginning of the exposure, with a sampling rate of 250 per second.

3.2.1   Ziehm Vision RFD

On the Ziehm equipment, set up as in figure 2.1, we measured the irradiation for DSA fluoroscopy with 25, 12.5, 8 and 4 frames per second and for both traditional and CO_2 program. Figure 3.4 shows the dose-rate waveforms for the traditional DSA fluoroscopy, while figure 3.5 represents those for the CO_2-specific program.

We found that, with the considered set-up, the equipment irradiates with the same parameters for all settings, as shown in table 3.4.

	ICM			**CO$_2$**		
fps	kVp	mA	ms	kVp	mA	ms
25	67	58.8	20	67	58.8	20
12.5	67	58.8	20	67	58.8	20
8	67	58.8	20	67	58.8	20
4	67	58.8	20	67	58.8	20

Table 3.4: Emission parameters obtained on Ziehm Vision RFD.

The pulse lengths were determined by fitting a pulse wave to the waveforms, as can be seen in figure 3.3: in this case we have 20 ms long pulses with intervals of 60 ms, thus 12.5 pulses per second.
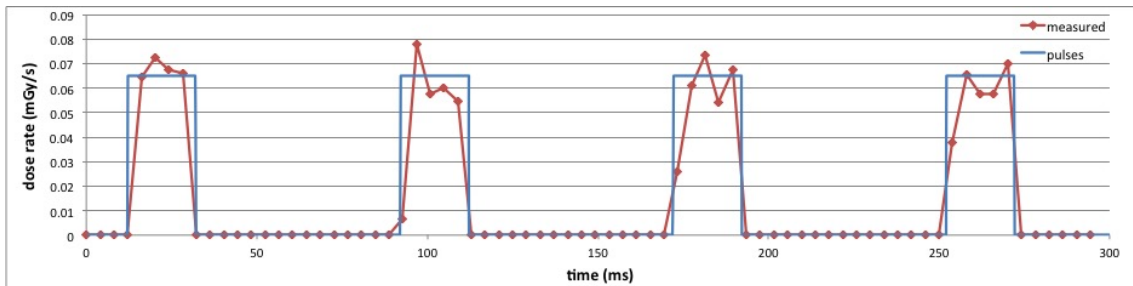
Figure 3.3: A close-up of some pulses from the traditional DSA acquisition with 12.5 fps on Ziehm equipment, with a pulse wave fit.

In the dose rate graphs we can clearly distinguish two emission phases: the first phase is the acquisition of the mask image, while the real DSA acquisition starts after it. It is worth noting that the mask is always acquired with 25 frames per second, regardless of the selected pulse rate. Of all the considered systems, this is the only one in which this happens.

An interesting remark can be made on the 12.5 fps sequence for CO_2 (second graph on figure 3.5). As this was actually the first acquisition on this equipment, we can observe the automatic exposure control at work: at the beginning, the tube voltage is clearly changing, and the mask acquisition starts only after the voltage has stabilized at around 67 kV.
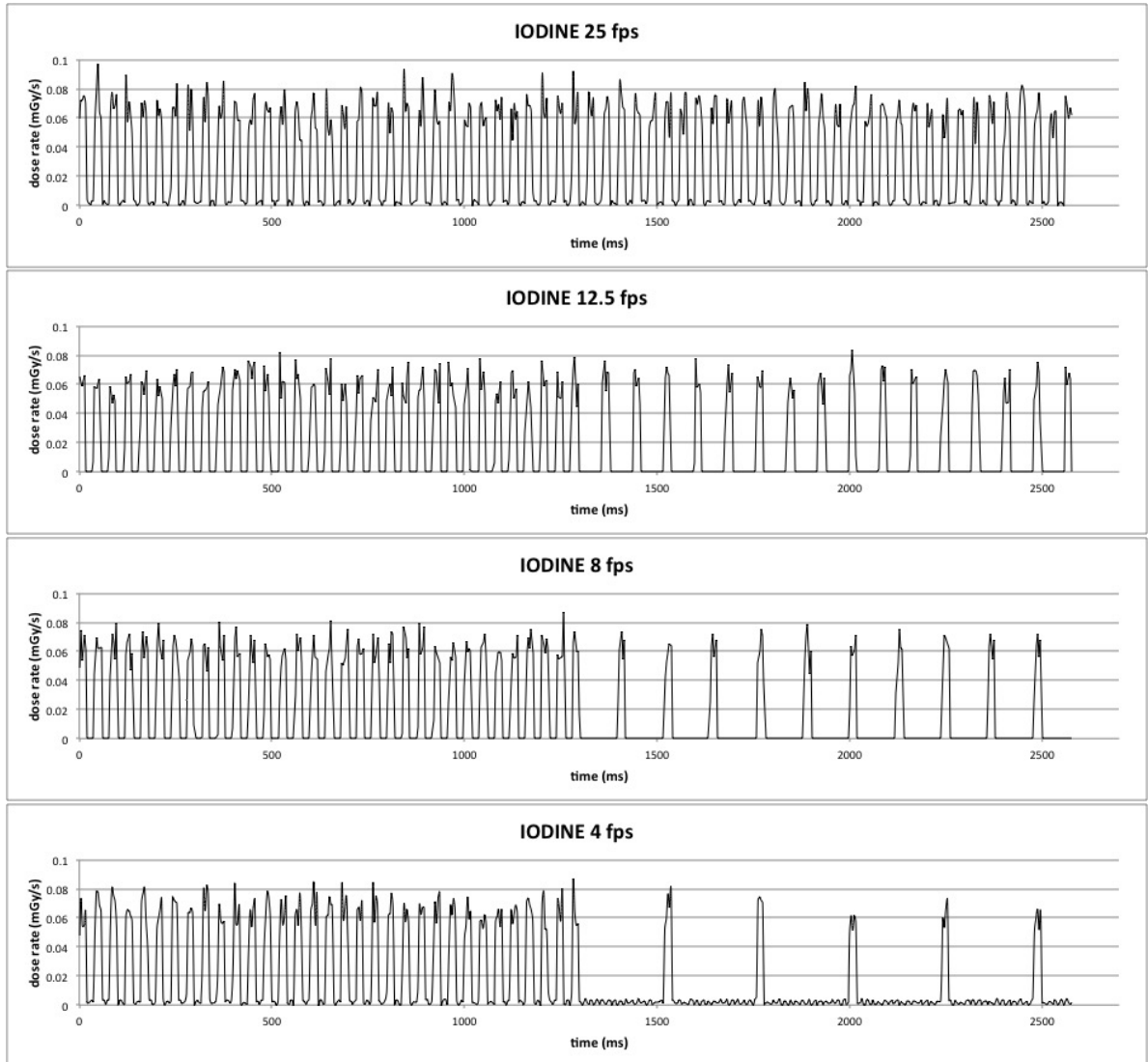
Figure 3.4: Dose rate waveforms for traditional DSA measured on Ziehm Vision RFD with 25, 12.5, 8 and 4 fps.
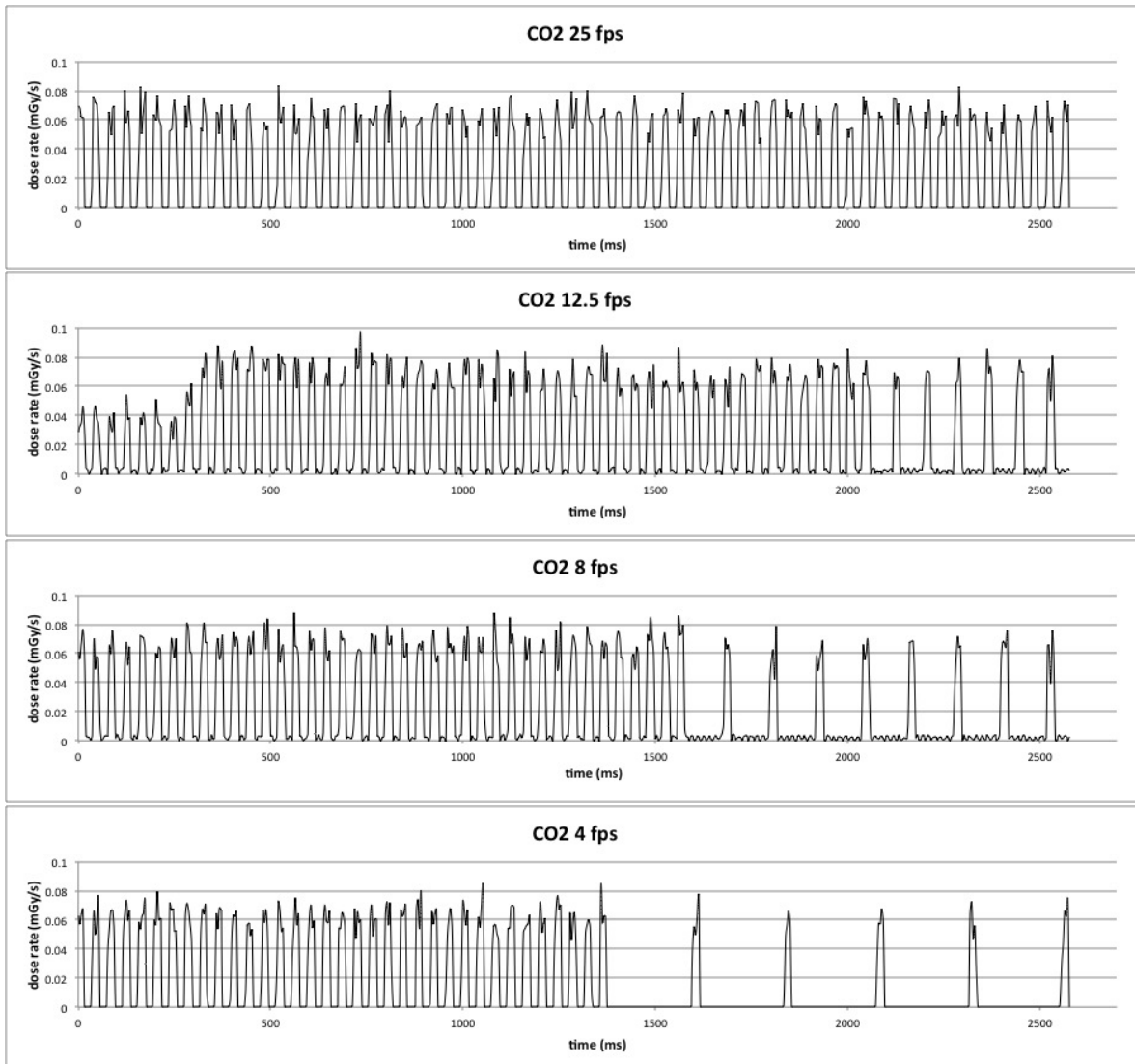
Figure 3.5: Dose rate waveforms for CO_2 DSA measured on Ziehm Vision RFD with 25, 12.5, 8 and 4 fps.

3.2.2   Siemens ANGIOSTAR

Since the Siemens ANGIOSTAR equipment does not have a CO_2-specific program, we just analyzed its emission with the DSA fluoroscopy program for traditional contrast agents, with 6 and 4 frames per second. The set up is shown in figure 2.2. The emission parameters are shown in table 3.5 , and the obtained dose-rate waveforms are shown in figure 3.6.

Looking at the waveforms we can see no clear phases as in the Ziehm equipment, hence we infer that the mask is acquired at the pulse rate selected by the operator.

		ICM	
fps	kVp	mA	ms
6	71	237	60
4	70	302	48

Table 3.5: Emission parameters obtained on Siemens Angiostar.
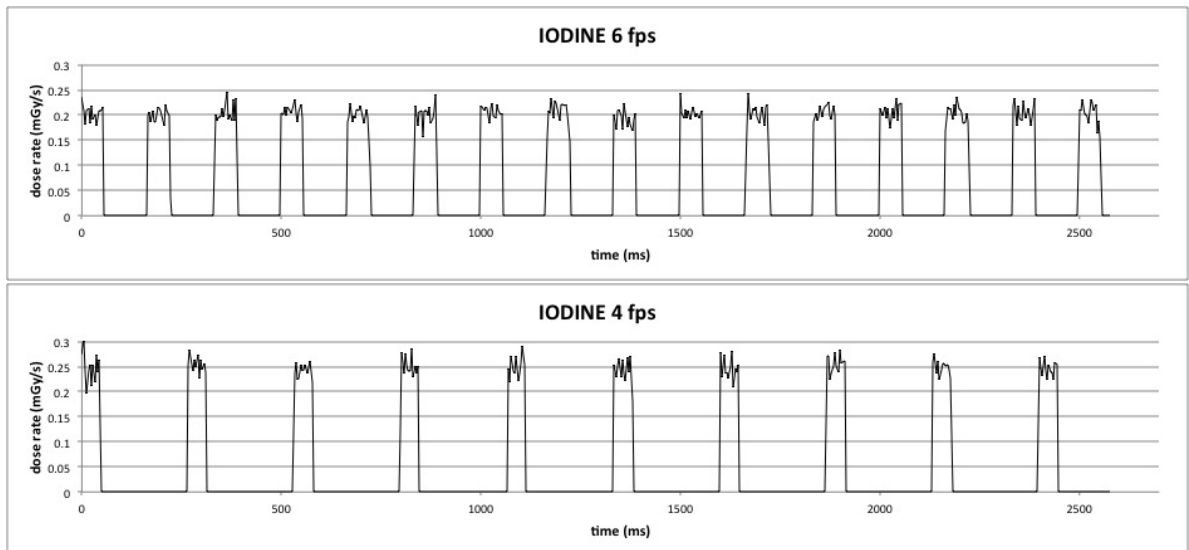
Figure 3.6: Dose rate waveforms for traditional DSA measured on Siemens ANGIOSTAR with 6 and 4 fps.

3.2.3 GE Innova IGS

The same measurements were performed on the GE equipment, set up as shown in figure 2.3, with pulse rates 7.5 and 4 frames per second. The dose-rate waveforms for the traditional DSA fluoroscopy are shown in figure 3.7, while figure 3.8 represents those for the CO_2-specific program.

As in the Ziehm equipment, even here we found no actual difference between the traditional DSA and the CO_2 DSA programs. In this case, however, the emission parameters changed for different pulse rates (table 3.6).

Once again we can see no clear phases in the waveforms, thus the mask is acquired at the selected pulse rate.

fps	ICM			CO_2		
	kVp	mA	ms	kVp	mA	ms
7.5	83	144	42	83	144	42
4	81	160	42	81	160	42

Table 3.6: Emission parameters obtained on GE Innova IGS.
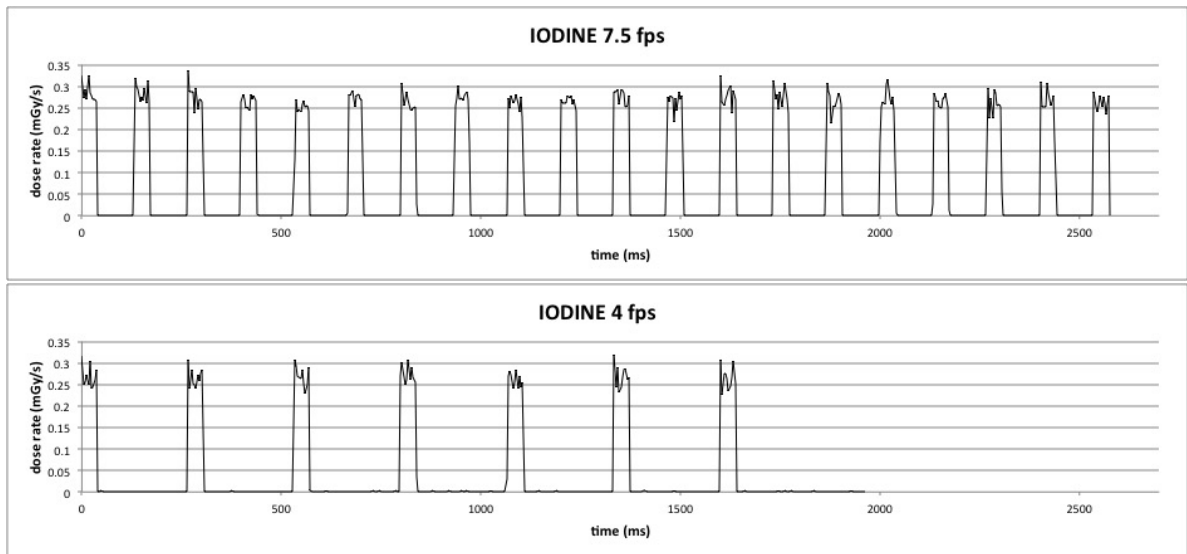
Figure 3.7: Dose rate waveforms for traditional DSA measured on GE Innova IGS with 7.5 and 4 fps.
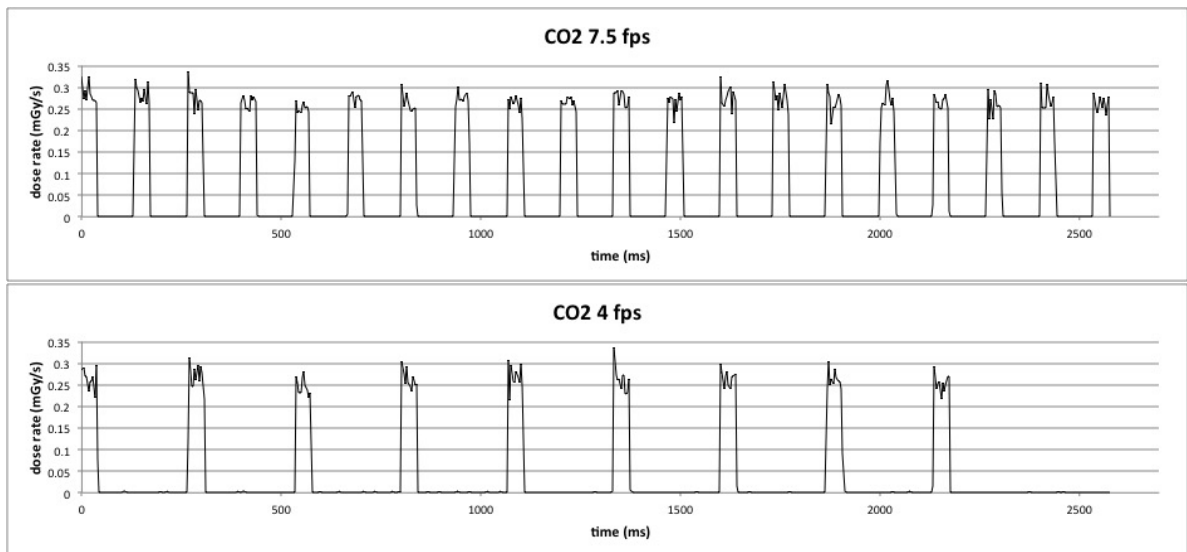
Figure 3.8: Dose rate waveforms for CO_2 DSA measured on GE Innova IGS with 7.5 and 4 fps.

3.3   Results comparison

The first evident result is that for both the Ziehm and the GE equipment, there was no difference whatsoever in the irradiation parameters between the traditional contrast media DSA and the CO_2-specific DSA protocols.

Table 3.7 presents the emission parameters of the two apparatus for both protocols, at a frame rate of 4 fps.

(4 fps)	ICM			CO$_2$		
	kVp	mA	ms	kVp	mA	ms
Ziehm	67	58.8	20	67	58.8	20
GE	81	160	42	81	160	42

Table 3.7: Emission parameters for ICM and CO_2 on Ziehm and GE, for 4 fps.

Comparing our measures, we can observe how the three fluoroscopes choose different parameters for the same set-up. We choose to analyze in particular the results obtained for a frame rate of 4 fps, as it is present in all of the equipment.

Table 3.8 shows a direct comparison of the emission parameters.

	Ziehm	Siemens	GE
kVp (kV)	67	70	81
Current (mA)	58.8	302	160
Pulse (ms)	20	48	42

Table 3.8: Comparison of the emission parameters for a frame rate of 4 fps.

The corresponding emitted X-ray spectra for a single pulse were simulated with the SpekCalc software (figure 3.9), and table 3.9 indicates their mean features. It is immediately clear that the three equipment administer very different doses for a single frame.

The photon density produced by the Ziehm equipment is significantly lower than the other equipment, and this is attributable to its less powerful generator. In fact, it uses the lowest voltage of the three fluoroscopes, the lowest current (less than one fifth of the one set by Siemens), and it has the shortest pulse (less than half of the others).
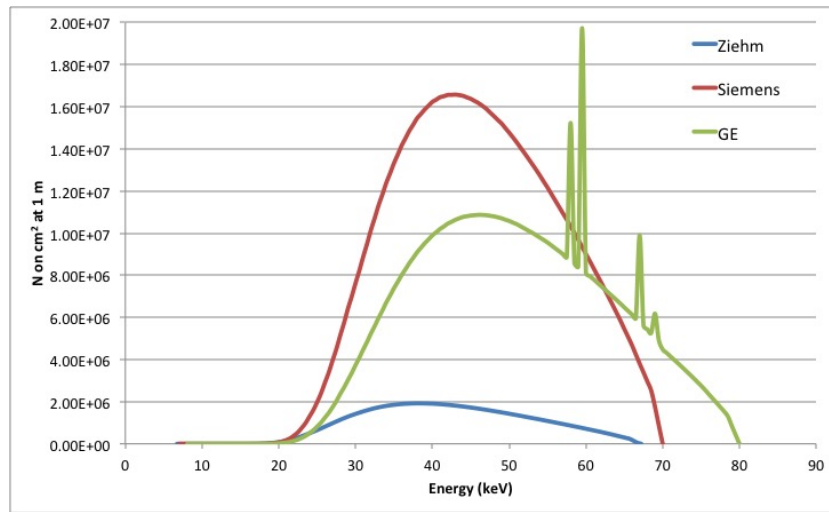
Figure 3.9: Simulated spectra for the three fluoroscopes, for 4 fps.

	Ziehm	Siemens	GE
HVL (mmAl)	3.4	4.4	5.3
Mean energy (keV)	42	46	51
Peak energy (keV)	38	42	46

Table 3.9: Characteristics of the analyzed spectra.

Siemens equipment uses a similar voltage, but with an elevated current and long pulse lengths (48 ms for 4 fps, 60 ms for 6 fps). Due to a higher filtration, its mean energy is higher than the Ziehm spectrum.

On the other hand, the GE fluoroscope sets a higher tube voltage, combined with an added Cu filtration.

Another important difference is the mask acquisition process. While Siemens and GE DSA programs execute the mask acquisition at the frame rate selected for the actual image acquisition, Ziehm uses the same high frame rate setting (25 fps) in any case. This might be done with the intent of obtaining a good mask image, to make up for the lower image quality obtainable with its limited power.

CHAPTER 4

Discussion

Along with the risk of air contamination and the technical difficulties of injecting a gaseous contrast material, one of the most common disincentives to the diffusion of CO_2 DSA in clinical practice is the concern about the administered dose. Considering that CO_2 provides less contrast than traditional ICM, in fact, it is generally believed that CO_2 DSA requires a higher dose than traditional angiographies.

To study the dosimetric aspects of CO_2 DSA, we decided to start by analysing how different fluoroscopy equipment set their irradiation conditions for this procedure.

Due to the characteristics of this contrast medium, we expected to find that equipment with CO_2-specific protocols would elevate the administered dose so as to make up for the lower image contrast.

Our results on two different machines (see table 3.7), however, show that the irradiation parameters were left completely unchanged between the traditional and CO_2 angiographic programs. This leads us to think that these CO_2 protocols do not operate on the X-ray emission, but only differ on an image manipulation level to enhance the obtained results.

These measures disprove the hypothesis that, on currently employed equipment, CO_2 angiography is intrinsically more dose-heavy than traditional DSA. For the present state of affairs, therefore, the problem of dose evaluation for CO_2 DSA procedures can be assimilated to the evaluations for traditional angiography, which have been widely discussed in literature.

51

The only parameter that could lead to an actual increment of patient dose is an augmented fluoroscopy time. This increment, if indeed present, might be due to the clinical staff's lack of experience with CO_2 injection and its technical difficulties, therefore requiring multiple repetitions of the acquisitions.

The emission parameters are set by the automatic exposure control system of the respective equipment, and their choice is a trade-off between administered dose and image quality. These parameters are generally optimized for traditional ICM. However, CO_2 is quite different from traditional contrast media for both X-ray absorption characteristics, such as the absence of a K-edge (figure 1.2), and for its dynamical and mechanical characteristics.

Therefore, the next question we addressed was whether the irradiation parameters were left unchanged from the traditional protocols for reasons of technical and economical convenience (e.g. a new emission protocol requires development funds and, moreover, an increase of maintenance complexity and costs), or whether they were the result of a CO_2-specific optimization process (e.g. changes in emission parameters did not give significant improvement of the obtainable images).

We believe that there is room for further researches and improvements on the choice of the optimal emission parameters for CO_2 DSA. In fact, even in the case of the widely-studied traditional contrast media, different equipment use different parameters.

Emission spectra for DSA are traditionally set considering the use of iodinated contrast media, hence they try to maximize the emission at energies corresponding to a higher iodine-tissue contrast. Considering that CO_2 does not have such limits, as it doesn't have a K-edge, and considering that modern flat panel detectors have wider dynamical ranges than traditional systems, higher tube voltages could be taken into consideration. In fact, this might give a better image quality, as photon fluence increases with the square of the voltage, while reducing the dose absorbed by the patient. The use of higher voltages would also represent an advantage for less powerful equipment, because reaching the same photon fluence by increasing the tube current would require much more power (as photon fluence is roughly $\propto$ kVp$^2 \cdot$ mAs).

Other parameters that could be discussed are the frame rate and the pulse length. Due to its physical properties, long pulse times were usually considered advisable for CO_2 DSA protocols, as the main interest did not lay in the imaging of the single bubbles, but in obtaining an image of a contrail of bubbles, realized by averaging over the length of the pulse.

Since modern fluoroscopes can perform complex image manipulations

without significant time lag, new protocols could be taken into consideration. For example, we could evaluate whether acquiring with higher frame rates and shorter pulse lengths, and then stacking the resulting images, could give an interesting or better outcome. More complex stacking algorithms could be tested, e.g. a thresholded algorithm that emphasizes the bubble signal by adding where the signal exceeds a certaing threshold, while averaging if it doesn't.

The transit of CO_2 bubbles inside the vessels could be very fast, thus it might be captured in just a few of the images. In this case, a non-discriminating stacking of all the acquired photograms does not represent the best solution, and a selective addition of the interesting imaged would be advisable. This process could even be implemented as an automatic system, for example by selecting a ROI around the vessel and only stacking the images in which this ROI has a change of contrast.

An important consideration on patient dose should also be made. As already stated, the patient dose for diagnostic and interventional procedures should be kept as low as reasonably achievable, based on a careful risk-benefit evaluation. In some clinical cases, however, it is clear that the minimization of dose is secondary to the need of good angiographic images. This is the case of the growing number of senior patients with relatively short life expectancy, serious vascular diseases with a concrete risk of gangrene, and with risk factors for contrast medium nephrotoxicity. For such patients CO_2 DSA could be the only possibility of intervention, and therefore an eventual increase in administered dose would be negligible when compared to the clinical benefits.

CHAPTER 5

Conclusions

The starting point of this work was the interest in the dosimetric aspects of peripheral digital subtraction angiographies using CO_2 as contrast medium.

Angiographic procedures are of growing importance due to the increase of patients with vascular conditions, a rising fraction of which also has renal diseases or other risk factors for traditional iodinated contrast media. In this perspective, CO_2 DSA is considered a valid alternative to traditional DSA. One of the main concerns with this technique is a possible increase in patient dose due to the lower contrast provided by carbon dioxide.

Analyzing the emission parameters for different fluoroscopic equipment, we found that there was no difference at all between the traditional and the CO_2-specific DSA protocols. Therefore there is no evidence that, with currently employed fluoroscopes, CO_2 DSA would administer higher doses than traditional DSA.

Considering the clinical advantages and the increasing degree of attention on this alternative contrast medium, we deem it appropriate to take into consideration an optimization of the emission parameters for the specific case of CO_2. In fact, the choice of the emission parameters in present apparatus is optimized for the use of iodinated contrast media, and might not represent the best choice for CO_2.

In addition to the emission parameters optimization , this work suggests many possible future developments.

For example, fluoroscopic equipment could be studied with more complex phantoms, with inserts containing the two contrast media. The use of dynamical phantoms might allow a better analysis of the imaging of moving CO_2 bubbles.

A measurement campaign for patient dose in traditional and CO_2 DSA procedures, with particular emphasis on the fluoroscopy times, could also provide interesting results. This would allow not only a comparison of the two procedures, but might lead to the assessment of diagnostic reference levels.

Bibliography

[1] Workshop on Efficacy and Radiation Safety in Interventional Radiology (1995: Neuherberg, Germany). Efficacy and radiation safety in interventional radiology. Geneva : World Health Organization, 2000.

[2] Sherry R. G., Anderson R. E., Kruger R. A., Nelson J. A. (1983). Real-time digital subtraction angiography for therapeutic neuroradiologic procedures. American journal of neuroradiology, 4(6), 1171-1173.

[3] Briguori C. La selezione e l'impiego ottimale del mezzo di contrasto. G Ital Cardiol 2009, 10(2), 79-87.

[4] Morcos SK, Thomsen HS (2001). Adverse reactions to iodinated contrast media. European radiology, 11(7), 1267-1275.

[5] Powe N. R., Moore R. D., Steinberg E. P. (1993). Adverse reactions to contrast media: factors that determine the cost of treatment. AJR. American journal of roentgenology, 161(5), 1089-1095.

[6] Lautin E. M., Freeman N. J., Schoenfeld A. H., Bakal C. W., Haramati N., Friedman A. C., Haramiti N. (1991). Radiocontrast-associated renal dysfunction: a comparison of lower-osmolality and conventional high-osmolality contrast media. American journal of roentgenology, 157(1), 59-65.

[7] Eisenberg R. L., Bank W. O., Hedgock M. W. (1981). Renal failure after major angiography can be avoided with hydration. American Journal of Roentgenology, 136(5), 859-861.

[8] Kerns S. R., Hawkins Jr I. F. (1995). Carbon dioxide digital subtraction angiography: expanding applications and technical evolution. AJR. American journal of roentgenology, 164(3), 735-741.

[9] Cho K, Hawkins IF , eds. (2013). Carbon dioxide angiography: principles, techniques, and practices. CRC Press.

[10] Patel BN, Kapoor BS, Borghei P, Shah NA, Lockhart ME (2011). Carbon dioxide as an intravascular imaging agent: review. Current problems in diagnostic radiology, 40(5), 208-217.

[11] Oliva V. L., Denbow N., Thérasse É., Common A. A., Harel C., Giroux M. F., Soulez, G. (1999). Digital subtraction angiography of the abdominal aorta and lower extremities: carbon dioxide versus iodinated contrast material. Journal of vascular and interventional radiology, 10(6), 723-731.

[12] Corazza I., Rossi P. L., Feliciani G., Pisani L., Zannoli S., Zannoli R. (2013). Mechanical aspects of CO2 angiography. Physica Medica, 29(1), 33-38.

[13] Johns H. E., Cunningham J. R. (1983). The Physics of Radiology 4th edn (Springfield, IL: Thomas).

[14] Dance D.R., Christofides S., Maidment A.D.A., McLean I.D., Ng K.H (2014). Diagnostic Radiology Physics: A Handbook for Teachers and Students (Vienna : International Atomic Energy Agency)

[15] Bushberg J. T., Seibert J. A., Leidholdt E.M., Boone J. M. (2002). The essential physics of medical imaging. Lippincott Williams & Wilkins.

[16] Holmes D. R., Laskey W. K., Wondrow M. A., Cusma J. T. (2004). Flat-panel detectors in the cardiac catheterization laboratory: Revolution or evolution—what are the issues?. Catheterization and cardiovascular interventions, 63(3), 324-330.

[17] Spahn M. (2005). Flat detectors and their clinical applications. European radiology, 15(9), 1934-1947.

[18] Seibert J. A. (2006). Flat-panel detectors: how much better are they?. Pediatric radiology, 36(2), 173-181.

[19] Nickoloff E. L. (2011). AAPM/RSNA physics tutorial for residents: physics of flat-panel fluoroscopy systems: survey of modern fluoroscopy imaging: flat-panel detectors versus image intensifiers and more. Radiographics, 31(2), 591-602.

[20] ICRP, 2007. The 2007 Recommendations of the International Commission on Radiological Protection. ICRP Publication 103. Ann. ICRP 37 (2-4).

[21] Ferrari P., Venturi G., Gualdrini G., Rossi P. L., Mariselli M., Zannoli R. (2010). Evaluation of the dose to the patient and medical staff in interventional cardiology employing computational models. Radiation protection dosimetry, ncq145.

[22] Stecker M.S. et al. for the SIR Safety and Health Committee and the CIRSE Standards of Practice Committee (2009). Guidelines for Patient Radiation Dose Management. Journal of Vascular and Interventional Radiology, 20(7), S263-S273.

[23] I.A.E. (2013). Tube Documentation - RTM70H, I.A.E. Spa, MI.

[24] GE Healthcare (2012). Performix 160A X-Ray Tube Assembly - Operating Documentation.

[25] RTI Electronics AB (2004). Barracuda User's Manual - Version 1.4A. Molndal.

[26] RTI Electronics AB (2004). oRTIgo 2002 User's Manual - Version 5.4A. Molndal.

[27] IEC normative 61267 : 2005-11

[28] Poludniowski G. G., Evans P. M. (2007). Calculation of x-ray spectra emerging from an x-ray tube. Part I. Electron penetration characteristics in x-ray targets. Medical physics, 34(6), 2164-2174.

[29] Poludniowski G. G. (2007). Calculation of x-ray spectra emerging from an x-ray tube. Part II. X-ray production and filtration in x-ray targets. Medical physics, 34(6), 2175-2186.

[30] Poludniowski G., Landry G., DeBlois F., Evans P. M., Verhaegen F. (2009). SpekCalc: a program to calculate photon spectra from tungsten anode x-ray tubes. Physics in medicine and biology, 54(19), N433.

[31] Chen S. C., Jong W. L., Harun A. Z. (2012). Evaluation of x-ray beam quality based on measurements and estimations using SpekCalc and IPEM78 models. The Malaysian journal of medical sciences: MJMS, 19(3), 22.